NASA TECHNICAL NOTE

NASA TN D-5360

NASA TN D-5360

ABSOLUTE RADIOMETERS FOR USE IN BALLISTIC-RANGE AND SHOCK-TUBE EXPERIMENTS

by Roger A. Craig and William C. Davy

Ames Research Center
Moffett Field, Calif.

NATIONAL AERONAUTICS AND SPACE ADMINISTRATION • WASHINGTON, D. C. • OCTOBER 1969

1. Report No. NASA TN D-5360	2. Government Accession No.	3. Recipient's Catalog No.
4. Title and Subtitle ABSOLUTE RADIOMETERS FOR USE IN BALLISTIC-RANGE AND SHOCK-TUBE EXPERIMENTS		5. Report Date October 1969 6. Performing Organization Code
7. Author(s) Roger A. Craig and William C. Davy		8. Performing Organization Report No. A-3192
9. Performing Organization Name and Address NASA Ames Research Center Moffett Field, Calif. 94035		10. Work Unit No. 129-01-02-08-00-21 11. Contract or Grant No.
12. Sponsoring Agency Name and Address National Aeronautics and Space Administration Washington, D. C., 20546		13. Type of Report and Period Covered TECHNICAL NOTE 14. Sponsoring Agency Code

15. Supplementary Notes

16. Abstract

This report is a discussion of the design, calibration, and use of radiometers to measure absolute spectral emission in ballistic-range and shock-tube experiments. These radiometers are characterized by a frequency response and a dynamic range sufficient to span the widely different frequencies and intensities of calibration and experiment sources. Radiometers discussed consist of a filter (transmission filter or monochromator), a detector (multiplier phototube or infrared photodiode), and a close-coupled amplifier. Response equations are developed that relate the test data to emission from a calibration standard. The principal problems of use of these radiometers (e.g., multiplier-phototube stability and saturation, infrared photodiode rise time and linearity, limiting noise, filter side-band transmission and standard lamp operation) are discussed.

Three currently operating ballistic-range and shock-tube applications at the Ames Research Center are described in detail.

17. Key Words Suggested by Authors	18. Distribution Statement
Radiometers Shock tubes Ballistic ranges Infrared detectors Multiplier phototubes	Unclassified - Unlimited

19. Security Classif. (of this report)	20. Security Classif. (of this page)	21. No. of Pages	22. Price*
Unclassified	Unclassified	59	$3.00

*For sale by the Clearinghouse for Federal Scientific and Technical Information
Springfield, Virginia 22151

TABLE OF CONTENTS

	Page
SUMMARY	1
INTRODUCTION	1
SYMBOLS	3
RADIOMETER REQUIREMENTS	4
Experimental Environment	5
Radiometer Components	5
Spectral elements	6
Detectors	7
Auxiliary electronics	9
RADIOMETER RESPONSE EQUATIONS	9
Response Equation	10
Calibration and Use of Radiometers	11
Filter-radiometer	11
Monochromator-radiometer	15
CALIBRATION TECHNIQUES	18
Absolute Spectral Standards	18
Tungsten lamps	19
Heated cavity	21
Monochromatic Sources	21
Observation of Calibration Signals	21
Techniques of Detector Operation	22
Multiplier phototubes	23
Solid-state infrared detectors	26
APPLICATIONS	29
APPENDIX A - MATHEMATICAL MODEL OF MONOCHROMATOR-RADIOMETER RESPONSE	34
RESPONSE EQUATION	34
Grating Monochromator	34
Prism Monochromator	38
APPENDIX B - AUXILIARY ELECTRONICS FOR MULTIPLIER PHOTOTUBES AND SOLID-STATE INFRARED DETECTORS	39
MULTIPLIER PHOTOTUBES	39
SOLID-STATE INFRARED DETECTORS	41
APPENDIX C - DETECTOR NOISE LIMITATIONS	43
MULTIPLIER PHOTOTUBES	43
SOLID-STATE INFRARED DETECTORS	46
ADVANTAGE OF MULTIPLIER PHOTOTUBES	48
IMPROVEMENT OF SIGNAL-TO-NOISE RATIO	50
APPENDIX D - STANDARD LAMP-CURRENT ACCURACY REQUIREMENTS	51
REFERENCES	55

ABSOLUTE RADIOMETERS FOR USE IN BALLISTIC-RANGE AND SHOCK-TUBE EXPERIMENTS

By Roger A. Craig and William C. Davy

Ames Research Center

SUMMARY

This report is a discussion of the design, calibration, and use of radiometers to measure absolute spectral emission in ballistic-range and shock-tube experiments. These radiometers are characterized by a frequency response and a dynamic range sufficient to span the widely different frequencies and intensities of calibration and experiment sources. Radiometers discussed consist of a filter (transmission filter or monochromator), a detector (multiplier phototube or infrared photodiode), and a close-coupled amplifier. Response equations are developed that relate the test data to emission from a calibration standard. The principal problems of use of these radiometers (e.g., multiplier-phototube stability and saturation, infrared photodiode rise time and linearity, limiting noise, filter side-band transmission and standard lamp operation) are discussed.

Three currently operating ballistic-range and shock-tube applications at the Ames Research Center are described in detail.

INTRODUCTION

One of the important phenomena of hypersonic flight is the radiation of energy from the vehicle flow field. Such radiation, by chemical species derived from the atmosphere (ref. 1) or by species that are products of the ablation process (refs. 2 and 3) can participate importantly in energy transport within the flow field. Additionally, this radiation is an important diagnostic tool for the study of chemical and thermodynamic processes that occur in the flow field. Several techniques have been developed for generating in the laboratory the high-temperature conditions that approximate the hypersonic flow field. Two of the most popular devices for this are the ballistic range (ref. 4) and the shock tube (ref. 5).

The development and calibration of radiometric instrumentation for use in ballistic ranges and shock tubes represent a major portion of the effort required to obtain trustworthy radiation data. Experimentation in either of these devices imposes constraints on the radiometer system that are somewhat unique. Applications to which a substantial portion of the standard literature is directed (e.g., astronomical) are characterized by very weak signals and long duration exposures (minutes to hours). Many other references are concerned with the detection of infrared sources rather than source strength measurement. In contrast to this, ballistic-range and shock-tube tests

characteristically have short test times (the order of tens of microseconds or less); hence, the radiometers must inherently be short-rise-time instruments. In addition, because calibration and testing usually represent radically different radiation-detector environments, the extrapolation of calibration data to the interpretation of test results must be done with great care. In particular, the experiment often requires measurements over an extreme range of intensities, from intense to weak, whereas calibration source intensity is limited to an often weak maximum; hence, instrument linearity and dynamic range must be known. Additionally, calibration is usually done in a continuous mode with a steady or modulated radiation flux, whereas the test produces a single, short duration, radiation pulse that occurs after the radiometer has experienced a period of dark quiescence; thus it is necessary to know the relationship between pulse and continuous mode operation. These are examples of but two of several problems that are encountered.

Many types of detectors used in ballistic ranges and shock tubes have been described in the literature. These can be categorized into two broad classes: thermal detectors and quantum detectors. The operation of thermal detectors depends on the absorbed energy modulating an intrinsic physical property of the detector (usually electrical) such as bimetallic junction potential, electrical conductivity, polarization, or capacitance. These detectors usually rely on a blackened surface to ensure uniform spectral response and are generally used to measure the total radiant power of the test event (ref. 6). Quantum detectors, (phototubes, multiplier phototubes, and solid-state detectors) on the other hand, employ phenomena that convert quanta directly into electrical current. Quantum detectors are much more sensitive than thermal detectors; see, for example, the figures of reference 7, chapter 10. However, because of the transitions that occur in quantum detectors, the spectral response is limited to wavelengths shorter than those corresponding to some threshold energy.

The purpose of this paper is to relieve a sometimes frustrating problem that is presented to the experimenter who has expertise in the problem being studied in the facility rather than in radiometric measurement techniques. Since it is often difficult and very time-consuming to decipher the standard radiometric literature, we will attempt here to present, in a concise and reasonably comprehensive form, the general notions required to design and use radiometric apparatus in a shock tube or a ballistic range. In addition, we will discuss the types of radiometers that are in general use in these facilities at the Ames Research Center. These radiometers consist of a detector (either a multiplier phototube or a cooled solid-state infrared detector), a spectral filter, a close-coupled amplifier, and a recording oscilloscope. The spectral filter is either some form of optical filter or monochromator.

Response equations are derived for radiometers that utilize optical filters or monochromators. The results of the mathematical analysis of the monochromator-radiometer allow variation of sensitivity, spectral coverage, and band-pass shape without recalibration. Also discussed are calibration techniques with emphasis on often troublesome points, such as multiplier-phototube stability, infrared detector rise time and linearity, limiting noise, filter side-band transmission, and standard lamp operation.

Three currently operating ballistic-range and shock-tube applications at Ames Research Center are described.

Appendix B, by Donald E. Humphrey, describes two amplifiers used in the radiometers discussed in the text.

SYMBOLS

A	radiometer aperture, cm^2
C	capacitance, F
d	monochromator reciprocal dispersion, μ/cm
$\mathscr{E}(\lambda)$	detector quantum efficiency, A/W
$E(\lambda,T)$	source spectral radiance, W/cm^2-μ
e	electron charge, 1.602×10^{-19} C
$F(\lambda)$	monochromator-radiometer sensitivity function, equation (A7)
$f(\lambda)$	normalized transfer function of monochromator-radiometer
$\mathfrak{G}$	ratio of absolute spectral flux to relative spectral flux, equation (7a)
G	radiometer electronic sensitivity, V/A
$\mathscr{K}$	monochromator-radiometer calibration constant, V-cm/W, equation (A8)
i	current, A
$\bar{i}$	mean detector current generated by test event, A
$\bar{i}_b$	mean detector current generated by the background radiation, A
i_ϕ	mean output current from detector, A
$H(\lambda)$	irradiance on the radiometer aperture, W/cm^2-μ
$\bar{H}(\lambda_o)$	equivalent average spectral irradiance from a continuum source, equation (5), W/cm^2-μ
$h(\lambda)$	relative spectral irradiance, W/cm^2-μ
$L(\lambda)$	standard source spectral irradiance, W/cm^2-μ
ℓ	monochromator slit height, cm

N_e	number of photoelectrons contained in a time-resolution interval
n_f	multiplier-phototube noise factor
$R(\lambda)$	detector spectral response, A-cm^2/W
$\Re(\lambda)$	radiometer spectral response, A-cm^2/W
s_1, s_2	monochromator entrance and exit slit widths, respectively, cm
s	monochromator indicated slit width, cm, equation (A10)
T	temperature, °K
$T(\lambda)$	spectral filter transmission
v	radiometer output signal, V
v_c	radiometer output in response to the calibration source irradiance, V
v_t	radiometer output in response to the test irradiance, V
$W(\lambda,T)$	Planck's function, W/cm^2-μ
$\bar{\varepsilon}$	total emissivity of tungsten
$\varepsilon(\lambda,T)$	emissivity of tungsten
Δf	electronic band pass, Hz
δ	monochromator indicated slit width correction, cm, equation (A10)
δ_t	measurement time interval, sec
λ	wavelength, μ
λ_o	wavelength at which radiometer has maximum sensitivity, or monochromator grating drive setting, μ
τ_r	electronic rise time: that is, time for 0.1 to 0.9 response to step function, sec
$\tau(\lambda)$	aggregate transmission of the internal components of a monochromator

RADIOMETER REQUIREMENTS

Prior to the discussion of calibration, it will be helpful to consider the experimental environment in which ballistic-range and shock-tube radiometers are expected to operate, and to describe the radiometer components,

since both determine to some extent the calibration procedures required. The predominant characteristics of typical experiments are (1) the short duration of the test event, and (2) the exceedingly wide dynamic range of the radiation intensities.

Experimental Environment

The time duration of the event and the time resolution required for interpreting the experimental data fix the rise-time requirements of radiometer systems. Typical high performance shock tubes provide flow times of uncontaminated test gas on the order of 10 μsec. However, the study of chemical kinetics requires that the nonequilibrium region following the shock be resolved, and this often requires radiometer rise times less than 0.1 μsec (ref. 8). Model launching devices used in contemporary ballistic-range testing are capable routinely of achieving model velocities in the range of 6 to 8 mm/μsec. Thus, to resolve the flow field of a 40-mm-long model flying at 8 mm/μsec into five parts requires rise times on the order of 1/2 μsec or less. It should be pointed out that there is generally some physical characteristic of the experiment that sets a limit to the time resolution of the data. For example, because of shock-wave curvature, it is the usual practice to record ballistic-range data only after the shock layer has moved fully into the radiometer view field. If this represents 1 mm of model travel, the shortest rise time required will be about 0.1 μsec. Excessively short rise times adversely affect the experiment precision, because high-frequency noise is admitted (see appendix C). Thus a radiometer design for a given experiment will have an optimum rise time lying between the limits discussed above.

Due to the wide variety of radiative phenomena that may be studied with various spectral resolutions in ballistic ranges and shock tubes, the experimental radiation intensities that are encountered vary over a wide range. In contrast, the standard sources of ultraviolet and visible radiation are of relatively low intensity so that the experimenter may be faced with the situation where the calibration and test event intensities are decades apart. For example, the radiometer irradiance was as high as 2.5×10^{-3} W/cm^2-μ at 0.25 μ during the tests of small (7-mm diameter) ballistic-range models reported in reference 2. The irradiance available for calibration is seen from figure 6 (to be subsequently discussed) to be only about 1 percent of this value. Hence, it is important to establish the dynamic range over which the radiometer responds linearly or, alternatively, to define precisely the nonlinear behavior of the radiometer between the test and calibration intensities.

Radiometer Components

A radiometer has three principal components: (1) a spectral filter that transmits only the spectral region over which the instrument is responsive, (2) a detector that converts the photon flux transmitted by the spectral element into an electrical current, and (3) an electronic output stage that converts the current generated by the detector into a suitable form, usually

a voltage that is recorded as an oscillogram. Auxiliary items, which may be attached to the radiometer or may be part of the ballistic range or shock tube, include field stops that limit the field of view of the radiometer and serve to reduce scattered radiation, and lens or mirror systems that might be used to increase the solid angle over which the radiometer collects radiation. When imaging optics are used before the aperture, the data reduction can become more involved. If only part of the beam gathered by the imaging system enters the aperture, the source must be positioned more accurately than when no imaging optics are used. If large solid angles are subtended from a volume source (e.g., the radiating region behind the shock wave in a shock tube), the view field may include gas over a wide range of thermodynamic conditions, further complicating data reduction. In a ballistic range, where the model flight-path position varies from test to test, the use of imaging optics may result in loss of data on an unacceptable fraction of the tests. Therefore, afocal systems should be used whenever possible.

Spectral elements.- The spectral element of the radiometer may be either an absorption filter that absorbs or an interference filter that reflects radiation of undesired wavelengths. An element that disperses the incident beam into its spectral components, such as a monochromator or a spectrograph, may also be used; the required spectral selection is then obtained by collecting the desired portion of the dispersed beam.

The use of filters is relatively inexpensive and allows a compact radiometer design, since the filter need be only as large as the active area of the detector. Absorption filters are available from several manufacturers and may be combined in series to obtain some control over the wavelength band pass and band center. It is often difficult to obtain narrow band passes in this manner, however; but multilayer dielectric interference filters may be manufactured to desired specifications. These filters are discussed in numerous standard texts (e.g., ref. 9). The band pass of an interference filter is a function of the incident angle of the transmitted beam, so that if the radiometer has a wide acceptance angle ($>10°$), this effect should be taken into account. Reference 10 contains a discussion of this effect.

Since filter-radiometers are of fixed band, and since their calibration can be somewhat laborious (as is discussed later in this report) the use of a monochromator or spectrograph as the spectral element may be considered if need for band-pass variability is anticipated. These devices are convenient since the band-pass width and center may be mechanically varied by adjusting slits and the position of the dispersing grating or prism. A grating monochromator with independently adjustable slits is particularly versatile since the band center of the exit beam is a nearly linear function of the angular position of the grating, and the band pass, as well as solid angle subtended by the radiometer, may be varied by adjusting the slits. Grating monochromators, however, have the property of transmitting higher orders, namely, wavelengths equal to the primary wavelength divided by integers. Hence, these higher orders must be blocked if the test event radiates, and the detector responds at these wavelengths. An absorption filter that blocks short wavelengths and passes long wavelengths is a convenient means of blocking higher orders. A wide assortment of these absorption filters is commercially available.

Radiometers employing monochromators or spectrographs are usually large compared to filter-radiometers because of the focal lengths of the internal optics required to give the instruments adequate spectral dispersion.

Detectors.- The choice of detectors for a radiometer design is controlled by several factors. Rise time, spectral sensitivity, and signal-to-noise ratio must be commensurate with experimental requirements.

Quantum detectors are of two classes: external and internal photo effect detectors. In the former, a photon incident on the sensitive area causes emission of an electron that is collected on an electrode held at a positive potential with respect to the photoemissive surface and processed as a current signal. In the latter, the electrons are excited only into the conduction band of the detector material.

Muliplier phototubes utilize the photoemissive effect of a semiconductor that forms the cathode of the tube; they are responsive in the ultraviolet, visible, and near infrared ranges out to approximately 1.2 μ (see refs. 11, 12, and 13 for a general discussion of multiplier phototubes).

The photon energy must be sufficient to cause cathode emission of an electron (i.e., to overcome the work function). There have not yet been developed cathode materials with work functions of sufficiently small value to be responsive at wavelengths longer than about 1.2 μ (ref. 11). Multiplier phototubes should always be considered for radiometric application since they are inherently very short rise-time devices and combine a large sensitive area with good quantum efficiency (i.e., the number of electrons emitted per incident photon). Maximum quantum efficiencies of 0.20 may be obtained for the visible region; however, values of 0.01 or less are typical for the infrared region.

An important advantage of multiplier phototubes is the current amplification that is achieved within the tube. This amplification arises from the impact of photoelectrons on the dynodes in the tube envelope, which then cause secondary electron emission. A potential of 50 V or more is used between dynodes for acceleration of electrons to energies necessary for good secondary electron yields. Current amplification of many decades is easily obtained by the use of a series of such dynodes. The advantage of this method of amplification is that it is achieved without the use of a load resistor; hence, the Johnson noise associated with any conventional amplifier is avoided. Also, adjusting the acceleration voltage across the dynodes adjusts the output signal to a convenient level for a wide range of radiant fluxes.

Multiplier phototubes possess finite limits to their dynamic-response range; the upper limit may be one of several saturation phenomena that occur within the tube. The nature and measurement of saturation is discussed in a later section of this report. The lower limit is due to noise. These quantum detectors are often used for very low level astronomical applications where the limiting noise is a "dark current" noise due to small currents generated within the tube even though the tube is in darkness. However, for pulse

operation such as is being considered here, the limiting noise is due to the statistical nature of the photon emission and photoelectron generation.

Noise limits of multiplier phototubes are discussed in appendix C where it is shown that the statistical noise is approximately $\sqrt{N_e}$, where N_e is the average number of photoelectrons generated during the resolution time interval. Statistical noise, as well as other noises, may be decreased by time averaging, such as by adding capacitance at the anode (see fig. 23). Time averaging decreases the high-frequency response of the radiometer or, equivalently, increases the rise time. Obviously, the rise time should not be increased beyond the time resolution requirements of the experiment. Neither should the rise time be significantly less than that required, since it would admit high-frequency noise to the signal without increasing the information content.

Of the various solid-state photodiodes responsive to infrared radiation (refs. 7, 14, 15), indium antimonide (InSb) cooled to 77° K (the temperature of liquid nitrogen) is commonly used for ballistic range and shock-tube experiments. These detectors are usually supplied mounted in the bottom of a small Dewar flask into which liquid nitrogen can be poured and retained. The detector view field is straight down through an infrared window (e.g., sapphire). These detectors have high sensitivity in the spectral range from 1 to 5 μ and thus complement the multiplier-phototube range. Optimum signal-to-noise ratio is obtained by operating this type of detector at zero volt bias (ref. 14). This requires some provision for bias control in the external circuitry, since the background photon flux can cause the detector to produce a substantial self-bias. When biasing these detectors, note that the rise time and sensitivity are functions of the voltage across the detector. Hence, these characteristics should always be measured for the bias condition at which the experiment is to be conducted.

There are shortcomings to InSb detectors compared to multiplier phototubes. Most have small active areas; this means that the radiometer will subtend a very small solid angle if the detector is used afocally. If a focusing lens is used, the radiometer design is somewhat complicated.

Another disadvantage is the generally low electrical-output level from the detector. External amplification is thus required, and the amplifier must have sufficient frequency response and dynamic range to allow comparison of calibration and test intensities. An alternative might be to use an amplifier of variable gain; this procedure is analogous to changing the voltage supplied to the multiplier-phototube dynodes. The quantum efficiency of the solid-state diode, which may be as high as 0.7 compared to photocathode efficiencies of 0.20 or less, slightly offsets the low noise advantage of the multiplier phototubes since less amplification is required of the solid-state diode current. However, the Johnson noise of the subsequent amplifier is always present in the solid-state diode radiometer output. It can be shown that if the vacuum photocathode efficiency is greater than about 0.002, the multiplier phototube may be expected to give a better signal-to-noise ratio for low level conditions of short duration irradiance. (See appendix C.)

Auxiliary electronics.- As mentioned above, internal amplification is obtained in multiplier phototubes through the use of secondary electron emission. Although individual voltage sources such as batteries may be used to provide acceleration potentials between dynodes, a more usual practice is to use a series of resistors to divide the voltage from a single high-voltage power supply. The dynode amplification is a very strong function of the voltage supplied to the divider series (see fig. 8 to be subsequently discussed); hence, it is important to obtain long term stability of the high-voltage power supply. Capacitors may also be used to stabilize dynode voltages when the tube is used in pulse-mode operation. The charges stored in the capacitors allow the dynode currents to exceed the divider current during the pulse.

The output stage of a multiplier phototube may consist of simply an anode load resistor that provides a ground path for tube current, thereby developing a voltage that can be recorded by an oscilloscope. The load resistor and the capacitance between the radiometer and oscilloscope constitute an RC network whose rise time may be the limiting factor in the system. This subject is discussed in detail in appendix B.

It is often desirable to include in the radiometer design a close-coupled amplifier to complement the gain of the multiplier phototube when the lowest level fluxes are being observed (see appendix B). The frequency response of such an amplifier must be high enough to accommodate the rise-time requirements of the experiment, and low enough, if it is ac coupled, to permit calibration of the radiometer. Calibration, to be discussed later, requires mechanical modulation of the calibration source, usually at a few hundred hertz, and the amplifier must handle signals of this frequency without attenuation. Note too that for test applications, the amplifier need only be unidirectional (i.e., required to amplify signals of only one polarity). Calibration conditions require the amplifier to be bidirectional if ac coupled. Appendix B describes an amplifier designed for this use.

As previously remarked, solid-state photodiodes should be operated with zero volt bias across the output terminals for optimum operation (rise time, sensitivity and signal-to-noise ratio) (ref. 14). If, to achieve this, the detector is operated into a low impedance, linear response will be attained, as seen from the equivalent circuit shown in figure 10. The nonlinear properties of the diode will not affect the current to the external circuit if the voltage across the parallel components is very low. The detector will exhibit a linear relationship between irradiance and the current passing through the external circuit. A close-coupled, low-input-impedance amplifier is described in appendix B that meets the above requirements and converts the photodiode current (usually very small) to a conveniently measured voltage.

RADIOMETER RESPONSE EQUATIONS

In the preceding section a radiometer was defined and described in terms of its component parts. Now the description is cast in terms of a mathematical model that describes, in functional form, the performance of a radiometer.

A response equation relating the output signal to absolute and spectral properties is given. The performance is then described in terms of this equation. Also, the terms that require measurement are discussed in two parts, first for a simple transmission filter-radiometer, and second for the more general case of a monochromator-radiometer.

Response Equation

In general, the radiometer output, v, may be expressed by the following equation:

$$v = G \int_0^\infty \Re(\lambda) H(\lambda) d\lambda \tag{1}$$

where

G electronic sensitivity of the system taken to be a constant, $\frac{V_{output}}{A_{detector}}$

$\Re(\lambda)$ spectral response of the radiometer, $\frac{A_{detector}}{(W/cm^2)_{incident}}$

$H(\lambda)$ spectral irradiance incident on the radiometer, $W/cm^2-\mu$

Since the unknown, $H(\lambda)$, appears in the integrand, the solution to equation (1) is not direct. Before proceeding further, we will discuss some mathematical aspects of solutions of the equation. This equation is generalized by allowing the output, v, to be a function of a variable, x. This variable would be continuous to represent a continuous wavelength spectrograph, or discrete to represent a system of many radiometers. The source spectral strength, $H(\lambda)$, then is related to the measured data, $v(x)$, by an equation of the form

$$v(x) = \int_0^\infty \Re(x,\lambda) H(\lambda) d\lambda$$

where x is an independent data variable, such as the position on the abscissa on a chart recorder output or an index number identifying the specific radiometer. This equation is a singular Fredholm integral equation of the first kind. Regardless of the narrowness of the nonzero region of $\Re(x,\lambda)$ for a specific x (i.e., spectral band pass of the instrumentation), a closed-form solution for $H(\lambda)$ would, in general, not be unique. In practice, a closed solution is not even possible since $v(x)$ and $\Re(x,\lambda)$ are not known analytically as functions of continuous variables. Even if they were actually given in analytical form, it would require considerable mathematical effort to find the inverse of the Fredholm equation to acquire a solution. This is usually not done; instead, some other technique of approximating $H(\lambda)$ is used, which may be as simple as taking $H(\lambda)$ to be a function of x instead of λ and removing it from the integral (as is sometimes done in film spectroscopy), or as elaborate as assuming a form for $H(\lambda)$ and warping it to synthesize the data. Examples of some of these techniques are included in this section. However, it should be understood that these techniques can only

produce approximations to the source spectral strength since they do not represent a mathematical solution of the Fredholm equation relating the radiometer output to the spectrum. For a discussion of techniques of numerically solving Fredholm equations, the reader is directed to reference 16, chapter 12.

Calibration and Use of Radiometers

It is possible to estimate the performance of a radiometer by evaluation of the terms in equation (1) from manufacturers' data or from the literature, but these values are nominal and not usually considered acceptable for absolute measurements. For accurate results, the radiometer itself must be used as a transfer device; that is, a device whose response to the incident flux from a test event is compared with its response to the incident flux from a source of known characteristics. The remainder of this section is a discussion of how the terms in equation (1) are measured by calibration and how the results are used to evaluate the test source strength from the radiometer output. The first case, that of a transmission filter-radiometer, follows.

Filter-radiometer.- The spectral response of a radiometer consisting of a transmission filter and a detector is given by the product of the filter transmission, $T(\lambda)$, and the spectral response of the detector, $R(\lambda)$. Thus equation (1) becomes

$$v = G \int_0^\infty R(\lambda)T(\lambda)H(\lambda)d\lambda \tag{2}$$

Writing a second expression for the response to a calibration source and dividing it into equation (2), we get a form of the response equation from which is easily seen the concept of a radiometer as a transfer device:

$$v_t = \left[\frac{\int_0^\infty R(\lambda)T(\lambda)H(\lambda)d\lambda}{\int_0^\infty R(\lambda)T(\lambda)L(\lambda)d\lambda}\right] v_c \tag{3}$$

where

v_t, v_c radiometer responses from the test and calibration, respectively, V

$L(\lambda)$ spectral irradiance on the detector from the calibration source, $W/cm^2-\mu$

It is apparent that before $H(\lambda)$ can be evaluated, v_t and v_c must be measured, the lower integral must be evaluated (by calibration of $R(\lambda)$, $T(\lambda)$, and knowledge of $L(\lambda)$), and the upper integral inverted so that the unknown does not appear in the integrand. Note that since the product $R(\lambda)T(\lambda)$ appears in both integrals, it is necessary to determine only the relative value of this product. The normalizing constants are factorable and thus cancel.

The wavelength range over which these measurements must be taken is a function not only of the filter and the detector, but also of the spectral irradiance, all of which are represented in the integrands. The experimenter

must ascertain that the wavelength limits of the integrals encompass the wavelengths containing important amounts of energy, and that the functions $R(\lambda)$, $T(\lambda)$, and $L(\lambda)$ are accurately represented.

The detector spectral response, $R(\lambda)$, can be determined by comparing it to that of another detector of known spectral response. It is of particular advantage to use a spectrally flat detector, such as a blackened thermocouple. The comparisons are made by utilizing an appropriate radiation source and a monochromator to provide radiation at various wavelengths. In the vacuum ultraviolet (ref. 17) and in the infrared at wavelengths longer than 6 μ (ref. 18), the conventional blackening materials used on thermocouples are not spectrally flat; hence, the spectral response must be measured or assumed. Reference 17 discusses the use of thermopiles as standards in the vacuum ultraviolet, and reference 18 discusses their use in the infrared. If the manufacturer's specifications for the radiometer detector indicate small variations in spectral sensitivity in the wavelength interval over which the response integrals are to be evaluated, then the experimenter may elect to use these specifications for $R(\lambda)$, depending on the accuracy sought in the results.

The filter is usually the element selected to limit the radiometer to the proper spectral range; for this reason, the degree to which it (1) accepts flux in this range, and (2) rejects the unwanted portion of the spectrum must be investigated. Often large errors can be introduced if the latter is ignored. The transmission of the spectral filter, $T(\lambda)$, is the ratio of the responses to nearly monochromatic flux of a radiometer with and without the filter positioned in the beam. The manufacturers of absorption or interference filters normally supply calibrations of filter transmission that have been obtained on double-beam recording spectrophotometers. However, they usually do not accurately determine the side-band transmission where complete blocking is desired. If there are contributions to the integrals of equation (3) in the regions of filter side-band transmission, then it is necessary to determine this transmission accurately. This problem can be illustrated by an example.

Consider the use of a tungsten lamp to calibrate an ultraviolet radiometer. The color temperature of the lamp filament (typically 2500° K) is such that the output is weak in the ultraviolet but very strong in the visible where many ultraviolet sensitive detectors respond. Thus, transmission of radiant power in the side-band region of the filter can dominate the signal. Figure 1 shows the measured transmission of a filter that was used in conjunction with a multiplier phototube. The resulting radiometer was used in tests described in reference 2. Note that the long wavelength side-band transmission remains above 10^{-4} for a substantial wavelength interval. (This feature is peculiar to this filter; some filters have been examined wherein transmission falls rapidly to very low values.) The use of the manufacturer's data for the detector response would be inadvisable in this case. The resulting integrand, $R(\lambda)T(\lambda)L(\lambda)$, evaluated for a tungsten ribbon filament calibration lamp at 2500° K color temperature and $R(\lambda)$ for an S-5 photocathode, shown in figure 2, is only slightly influenced by filter transmission in the region of primary transmission. If the side-band transmission of the filter were ignored, then it would be appropriate to let the

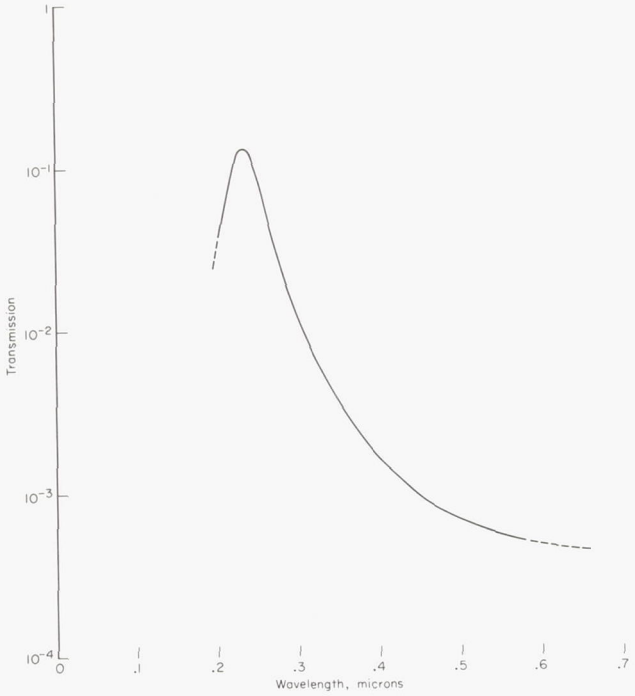

Figure 1.- Measured filter transmission.

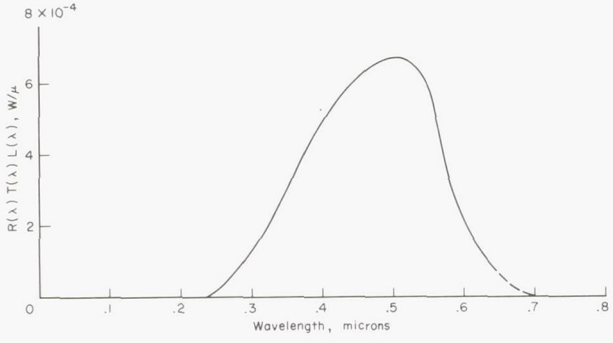

Figure 2.- Integrand of response equation for ultraviolet radiometer irradiated by tungsten standard source.

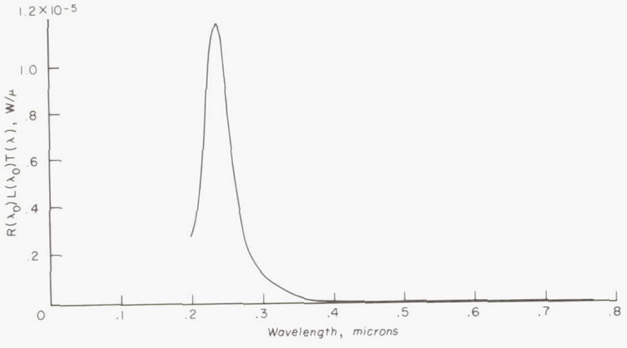

Figure 3.- Change of integrand shown in figure 2 when the side-band transmission of the filter is ignored.

detector response be constant and to approximate the standard lamp radiance by the value at the wavelength of maximum filter transmission, $L(\lambda_o)$. The denominator of equation (3) would then become

$$R(\lambda_o)L(\lambda_o)\int_o^\infty T(\lambda)d\lambda \qquad (4)$$

where the integrand is then the filter transmission.

Figure 3 is a plot of $R(\lambda_o)L(\lambda_o)T(\lambda)$, which is the integrand of the above expression multiplied by the product of the calibration lamp irradiance and the detector response at λ_o; it is then directly comparable to the integrand plotted in figure 2. (Note the ordinate scale change.) The ratio of the resulting integrals is then the error due to ignoring the filter side-band transmission, which is excessive in this case.

The case illustrated is a particularly adverse one, but it points out that certain combinations of filters and detector and radiant sources can produce undesired results. The above situation would change if a calibrated filter that transmitted ultraviolet and blocked visible radiation were employed with the calibration source to reduce the intensity of the long wavelength radiation.

The incident fluxes, $H(\lambda)$ and $L(\lambda)$, are supplied by the experiment and calibration sources, respectively. The calibration source is one of several devices discussed in the next section. The unknown, $H(\lambda)$, is directly relatable to the experiment source strength. Before this quanity can be related to the radiometer signal, the upper integral in equation (3) must be evaluated. This requires that some simplifying assumptions be made about $H(\lambda)$. Three special cases will be discussed:

(1) If the relative spectral shape of $H(\lambda)$ is not known, all that is possible to report are the results in terms of an average equivalent flux in the spectral response region of the radiometer. The equivalent average flux from a continuum source, defined as

$$\overline{H}(\lambda_o) = \frac{\int_o^\infty R(\lambda)T(\lambda)H(\lambda)d\lambda}{\int_o^\infty R(\lambda)T(\lambda)d\lambda} \tag{5}$$

is often reported, the argument, λ_o, indicating that the value should be identified with the region of maximum response of the radiometer. This flux is then given by

$$\overline{H}(\lambda_o) = \left(\frac{v_t}{v_c}\right)\left[\frac{\int_o^\infty R(\lambda)T(\lambda)L(\lambda)d\lambda}{\int_o^\infty R(\lambda)T(\lambda)d\lambda}\right] \tag{6}$$

In the event that the radiation is a continuum and can be well approximated by a constant plus an odd-ordered polynomial about λ_o, and, if the spectral response of the radiometer is symmetrical about λ_o, it can be shown that equation (6) is exact for this case, with $\overline{H}(\lambda_o)$ replaced by $H(\lambda_o)$, the value of the continuum at λ_o. It should be noted that if $L(\lambda)$ can be approximated by a constant value that is equal to its value at λ_o, equation (6) then reduces to the very simple form

$$\frac{\overline{H}(\lambda_o)}{\overline{L}(\lambda_o)} = \frac{v_t}{v_c} \tag{7}$$

(2) If the relative spectral irradiance is known, the integral can be evaluated by factoring out the unknown $\mathfrak{F}$, the ratio of the absolute spectral irradiance to the relative spectral irradiance, namely,

$$\mathfrak{F} = \frac{H(\lambda)}{h(\lambda)} = \left[\frac{\int_o^\infty R(\lambda)T(\lambda)L(\lambda)d\lambda}{\int_o^\infty R(\lambda)T(\lambda)h(\lambda)d\lambda}\right]\left(\frac{v_t}{v_c}\right) \tag{7a}$$

where $h(\lambda)$ is the relative spectral flux, $W/cm^2\text{-}\mu$.

(3) If $H(\lambda)$ is due to a single spectral line, or a narrow multiplet of lines (narrow compared to the band pass of the radiometer) and the line irradiance I is the desired quantity, only the response of the radiometer at the wavelength of the line (or lines), λ_L, is of interest. Equation (3) then reduces to

$$I = \left[\frac{\int_o^\infty R(\lambda)T(\lambda)L(\lambda)d\lambda}{R(\lambda_L)T(\lambda_L)}\right]\left(\frac{v_t}{v_c}\right) \tag{8}$$

where

$$I = \int_o^\infty H(\lambda)d\lambda, \ W/cm^2$$

Monochromator-radiometer.- If a monochromator replaces the transmission filter in the radiometer, the foregoing calibration description applies, provided the monochromator settings (wavelength drive and slit widths) are fixed. The ability to alter these settings, and thus change the filter properties of the monochromator, is the reason for using it as the filter element. The changes in filter properties are related in an orderly fashion, to the monochromator settings; hence, these change may be represented by appropriate functions in the response equation. We will discuss the response equation for a grating monochromator,[1] and the calibration of the various terms therein. The result is a description of the performance of a versatile radiometer whose sensitivity, spectral coverage, and spectral band-pass shape are variable over a wide range and are easily determined from the response equation and the calibration constants.

The response equation for a monochromator-radiometer, with internal optics that form a full-size image of the entrance slit at the exit slit and with individually adjustable entrance and exit slits, is given by equation (A6):

$$v = \mathscr{A}\,\mathrm{MIN}(s_1, s_2) \int_0^\infty F(\lambda) f(\lambda) H(\lambda)\, d\lambda \tag{9}$$

where

$\mathscr{A}$ — calibration constant (defined in appendix A), V-cm/W, that characterizes the system sensitivity

$\mathrm{MIN}(s_1, s_2)$ — function equal to the smaller of the two arguments, the entrance and exit slit widths, respectively, cm

$f(\lambda)$ — normalized transfer function as determined by the mechanical aspects of the monochromator. This is the term, analogous to the filter transmission, that characterizes the spectrally responsive region of the radiometer

$F(\lambda)$ — function proportional to the product of detector response and reflectivity (or transmission) of the internal optical surfaces. It is usually slowly varying with wavelength, and mainly indicates changes in absolute sensitivity of the radiometer as the grating is adjusted to different wavelength settings

$H(\lambda)$ — spectral irradiance at the entrance slit of the monochromator, $W/cm^2-\mu$

If the slit widths are fixed, then equation (9) reduces to equation (2), and the concept of a transfer standard remains.

---

[1]Prism monochromators are not discussed here. One could be used if the nonlinear dispersion is accounted for in the succeeding equations (see appendix A).

Equation (9) may be used to predict the performance of a monochromator-radiometer once the functions $F(\lambda)$, $f(\lambda)$ and the constant $\mathscr{A}$ are determined. If the side-band radiation is negligible or can be eliminated (by filtering, for example), some simplifications to equation (9) are possible. Since $F(\lambda)$ is a composite function determined by optical properties that generally do not vary rapidly with wavelength, it is possible to replace $F(\lambda)$ by its value at the center of the spectral band pass of the monochromator if the slits are adjusted to pass a narrow spectral interval. Thus, for this case, $F(\lambda)$ may be removed from the integral as the constant $F(\lambda_o)$. Further, if the radiation source may be similarly approximated, as would be the case for an incandescent filament, equation (9) reduces to[2]

$$v = \mathscr{A}\,\mathrm{MIN}(s_1,s_2)F(\lambda_o)L(\lambda_o)\int_o^\infty f(\lambda)\,d\lambda \tag{10}$$

where $L(\lambda_o)$ is, as earlier, the incident flux from the calibration source. From figure 21 (appendix A), we have

$$\int_o^\infty f(\lambda)\,d\lambda = \mathrm{MAX}(s_1,s_2)\,d \tag{11}$$

where MAX is defined analogously to the function MIN, and d is the reciprocal dispersion of the monochromator, μ/cm. Eliminating the integral from these two equations, we get

$$v = \mathscr{A}F(\lambda_o)L(\lambda_o)s_1s_2\,d \tag{12}$$

which is in a form suitable for determining $F(\lambda)$. For convenience, $F(\lambda)$ is defined to have a maximum value of unity, the normalizing constant being absorbed in the constant $\mathscr{A}$. It is necessary only to irradiate the entrance slit with a standard of spectral radiance, determine v as a function of the monochromator wavelength drive setting, λ_o, and deduce $F(\lambda)$ from the following equation:

$$F(\lambda) = F(\lambda_o) = \frac{v(\lambda_o)}{L(\lambda_o)}\left[\frac{L(\lambda_o)}{v(\lambda_o)}\right]_{MAX} \tag{13}$$

Figure 4 shows $F(\lambda)$ determined for radiometers utilizing multiplier phototubes and all-reflective monochromator optics. Three combinations of grating blaze wavelength and multiplier phototube cathode types are shown.

Any measurement taken during the determination of $F(\lambda)$ is also an absolute calibration and may be used to determine $\mathscr{A}$ directly by means of equation (12).

In appendix A, $f(\lambda)$ is derived as a function of the slit widths. However, this is for the region of primary transmission. There are, in

---

[2]The equation in this form is actually more general than is indicated by the conditions used in the derivation. This equation is exact if $f(\lambda)$ is symmetrical about λ_o, and the product $F(\lambda)H(\lambda)$ can be represented by a constant plus an odd-ordered polynomial about λ_o as mentioned before.

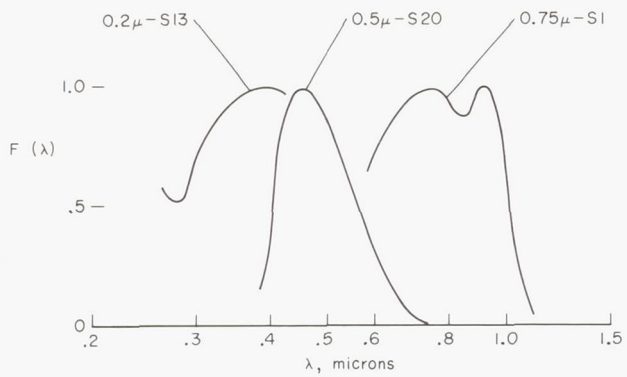

Figure 4.- F(λ) for various combinations of grating blaze wavelength and multiplier-phototube cathode types.

addition, regions of side-band transmission, because of the transmission of unwanted orders from the grating and because of optical imperfections within the monochromator. Unwanted orders are usually blocked with an optical filter. The remaining side-band transmission must be measured, however.

The procedure for measurement is different from that for a transmission filter, as the monochromator is not conveniently placed in and out of a radiation beam. Instead, the radiometer is irradiated by monochromatic radiation (from an atomic line source) near the wavelength of interest. The grating drive is then rotated to allow the transfer function to "scan" the fixed monochromatic line. This scanning generates the transfer function and provides quantitative measurements in the side-band regions. The transfer function shape is assumed not to be a function of grating drive position, which is to be expected for a normal-incidence grating monochromator. This technique is questionable when grazing incidence must be used. The response equation presumes that the slits used are wide enough so that the spectral band pass of the monochromator is determined solely from the mechanical sizes of the slits; that is, diffraction effects from the slit edges are negligible. The range of slit widths over which this assumption holds must be investigated.

Appendix A contains a description of this investigation of a 25-cm focal length monochromator with a reciprocal dispersion of 0.067 μ/cm. The result is that slit widths from 0.05 cm to 1.0 cm are usable, representing half-height bandwidths of 0.00335 μ to 0.0670 μ. Narrower settings would require separate measurement of $f(\lambda)$, as described above, for accurate results.

An example of such a measurement of narrow spectral band pass is given in reference 8 for a 25-cm focal length monochromator as above. The slits were set to achieve a trapezoidal spectral band-pass shape with a half-height width of 0.0029 μ.

As was the case with the filter-radiometer, the spectral irradiance, $H(\lambda)$, in equation (9) (the response equation) appears as the unknown in an integral equation. As before, we consider three special cases wherein $H(\lambda)$ is determined:

(1) The equivalent average incident flux from a continuum source is given by

$$\overline{H}(\lambda_o) = \frac{V}{\text{MIN}(s_1, s_2) \int_0^\infty F(\lambda) f(\lambda) d\lambda} \qquad (14)$$

which is simplified by means of equation (11) and the assumption $F(\lambda_o) = F(\lambda)$ to

$$\overline{H}(\lambda_o) = \frac{V}{\mathfrak{A} s_1 s_2 dF(\lambda_o)} \tag{15}$$

(2) Equation (9) may be used directly to solve for the absolute strength if the relative spectral shape of the source is known; namely,

$$\mathfrak{I} = \frac{V}{\mathfrak{A}\,\mathrm{MIN}(s_1, s_2) \int_o^\infty F(\lambda) f(\lambda) h(\lambda) d\lambda} \tag{16}$$

(3) When $H(\lambda)$ is a single line or a narrow multiplet of lines, and I, the line irradiance, is desired, equation (9) becomes

$$I = \frac{V}{\mathfrak{A}\,\mathrm{MIN}(s_1, s_2) F(\lambda_L) f(\lambda_L)} \tag{17}$$

where, as before, $I = \int_o^\infty H(\lambda) d\lambda$ and λ_L is the wavelength of the lines.

CALIBRATION TECHNIQUES

The use of the calibration apparatus, which is required for the various calibrations remarked upon earlier, has not yet been discussed. Confronting the experimenter is a variety of equipment that must be used carefully if the calibration results are to be trustworthy. The purpose of this section is to describe the apparatus used during calibration, and to discuss the techniques required for its proper use. Since calibration and testing usually represent radically different detector environments, we will emphasize techniques for determining corresponding differences in detector response.

Absolute Spectral Standards

The common absolute spectral emission standards are of two types: incandescent tungsten lamps for use in the 0.25 to 2.5-μ range, and heated cavities for use at longer wavelengths. For operation to wavelengths as short as 0.2 μ, short-lived tungsten lamps are available (ref. 19). The subject of absolute calibration in the vacuum ultraviolet is beyond the scope of this report. The sensitivity of such detectors, however, is obtained either by calculation from the physics of the detector or by extrapolation from a longer wavelength calibration and a known spectral response either of the detector in question or of a second detector, such as a blackened thermocouple. This calculation is then used as the standard (cf. refs. 17, 20, and 21).

Tungsten lamps.- It is possible to deduce the output from a section of the filament of a tungsten ribbon-filament lamp,[3] utilizing a calibrated pyrometer and tables of emissivity for tungsten given in reference 22. (Required for this use are values of brightness or color temperatures as functions of temperature for tunsten. These are given in reference 23.) Because of the uncertainties involved and the extra work required, it is usually more economical to purchase from one of several laboratories a calibrated standard lamp traceable to NBS primary standards.

Calibrated ribbon-filament lamps as described in reference 24 are available. These are normally used with calibrated mirrors that image the filament onto a small aperture to isolate a small portion of the filament. These mirrors are calibrated for reflectivity as described in reference 24. Also available are coiled-filament lamps, described in reference 25, which are calibrated in terms of the flux from the entire lamp onto a surface at a specified distance. These lamps are calibrated for absolute spectral irradiance as a function of wavelength and at a prescribed current, either ac or dc, through the lamp. Ribbon-filament lamps are operated at high currents for use in the ultraviolet. For longer wavelength use, the lamps are operated at a lower current to prolong their operating life. The long life of coiled-filament lamps is due to the presence of iodine within the envelope, the effect of which is discussed in reference 26.

When calibrated tungsten-filament lamps are used, a secondary or working standard is employed. This working standard is usually an identical lamp that has been compared to the calibrated standard and then used for routine calibrations; the function of the standard then is to check the performance of the working standard periodically. References 24 and 25 give instructions for operating these lamps. Not cited therein, but of interest, is the relationship between accuracy of the measurement of current through the lamp to accuracy of the measurement in radiant output. An approximate relationship is derived in appendix D for a tungsten-filament lamp at temperatures greater than 1000° K:

$$\frac{\delta i}{i} \cong (10^{-4})T\lambda \frac{\delta E(\lambda)}{E(\lambda)} \tag{18}$$

where

$\delta i/i$	fractional error in lamp current
$\delta E(\lambda)/E(\lambda)$	fractional error in lamp spectral radiance
λ	wavelength in microns
T	filament temperature, °K

---

[3]This procedure is not possible with a coiled-filament lamp, since the radiant interchange within the interiors of the coils causes the overall emissivity to be greater than that of tungsten and, hence, unknown.

For a wavelength of 0.25 μ and a temperature of 2500° K, the precision in current control must be 16 times greater than the desired precision of the spectral radiance. An additional need for precision arises because, in practice, there are three current measurements involved in the calibration of a radiometer: one for operation of the standard lamp, one for initial calibration of the working standard, and one for calibration of the radiometer. Hence, for calibration in this wavelength regime, it is necessary to measure the lamp current to the order of 0.1 percent. The lamp power supply at Ames Research Center includes a 0.01-percent line voltage regulator and a 0.1-percent current meter.

A typical calibration setup, consisting of a ribbon-filament lamp, a two-mirror train, a mechanical chopper, and aperture, is shown in figure 5. The two mirrors image the central portion of the filament on the aperture so that the radiometer receives only the best-characterized emission from the filament.

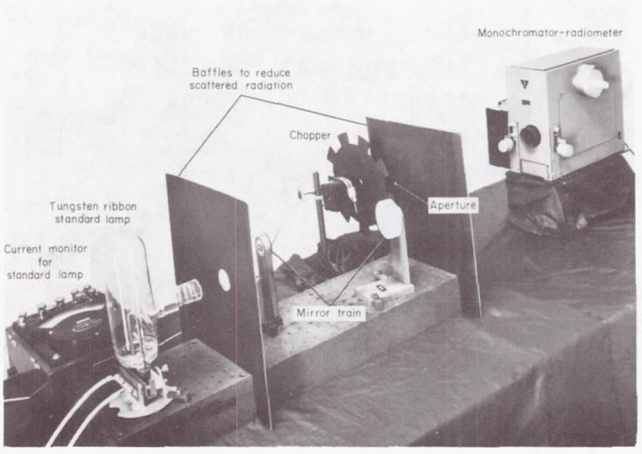

Figure 5.- Calibration apparatus using ribbon filament standard lamp.

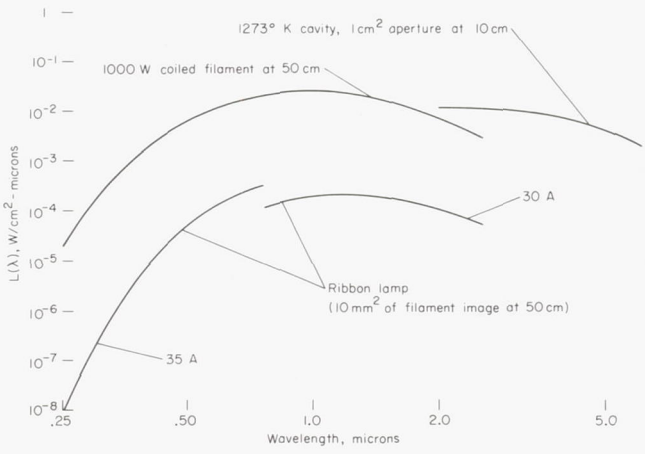

Figure 6.- Spectral irradiance produced by various standard sources.

If a coiled-filament lamp is to be used, the imaging mirrors and aperture are not used because of the spatial variation of emission from the coils. Instead, this lamp is placed next to the chopper so that the entire filament is seen by the radiometer. The chopper is used to permit ac coupling of the electronics system; it also permits synchronous amplification for improved signal-to-noise ratio. The radiometer being calibrated in figure 5 consists of a 25-cm focal length monochromator, multiplier phototube, and a close-coupled amplifier.

Figure 6 is a plot of the radiant flux at the radiometer aperture under typical calibration conditions from each of the two types of lamps. The working distance from the source (the coiled filament or the image of the ribbon filament) is 50 cm for both cases, and the area of the image aperture of the ribbon filament lamp is 0.1 cm^2. The ribbon-filament output is shown for the two currents, as mentioned above.

The spectral shape of the curves for the tungsten lamps indicates the desirability of using a calibrated filter, such as Corning No. 7-54, for calibrating in the ultraviolet. Such

a filter passes ultraviolet and blocks radiation at wavelengths longer than about 0.4 μ. Side-band radiation is thereby reduced at the source.

Heated cavity.- At wavelengths longer than 1 μ, it becomes practical to use heated cavities, designed to approximate a blackbody source. Several such devices are commercially available, complete with control apparatus to set and regulate the cavity temperature. Planck's equation (eq. (D2)) is then used to calculate the radiant output.

Shown also on figure 6 is the output from a commercial blackbody radiation source (Barnes Engineering Company, model 11-200) having a 1-cm^2 aperture and operating at 1273° K, which allows calibration of infrared detectors to longer wavelengths. The calculation was based on a distance of 10 cm from the aperture to the detector.

Monochromatic Sources

Often a radiation source is required to have almost monochromatic spectral qualitity, with little or no radiation at wavelengths outside of the central band. Sources of this type are required for filter transmission measurements and for monochromator transfer function measurements (appendix A). Various sources of such radiation are discussed below. In typical applications of these sources, only comparative measurements are made; hence, the absolute intensity need not be known, although it could be measured by a suitable radiometer.

A convenient source of near-monochromatic radiation is a monochromator irradiated with a continuum source to which blocking filters have been added to reduce side-band radiation to acceptable levels. The source is then variable in wavelength and is suitable for measuring primary transmission regions of filters. If the source strength is intense enough and the monochromator side-band blocking is adequate, the regions of secondary transmission may also be measured by this source.

Near-monochromatic sources of fixed wavelength may also be obtained with an atomic line source, such as a low-pressure mercury vapor or neon gas discharge tube, suitably filtered to isolate a line. Some of these sources produce very intense lines, which can be used for investigating filter side-band transmission at selected wavelengths. This kind of source was used to obtain the monochromator transfer function curves shown in figure 22 and discussed in appendix A.

Observation of Calibration Signals

If a radiometer is designed to operate in a continuous mode (dc), the output during calibration may be read directly on a suitable galvanometer-type meter. This is often done with slow response radiometers, such as camera light meters. Fast response radiometers, however, are usually not dc coupled, and require a modulated or pulsed calibration source. A modulated source is conveniently supplied by a mechanical chopper combined with any of the calibration standards mentioned. A camera shutter could be used to obtain a single short pulse and the output could be observed directly on an

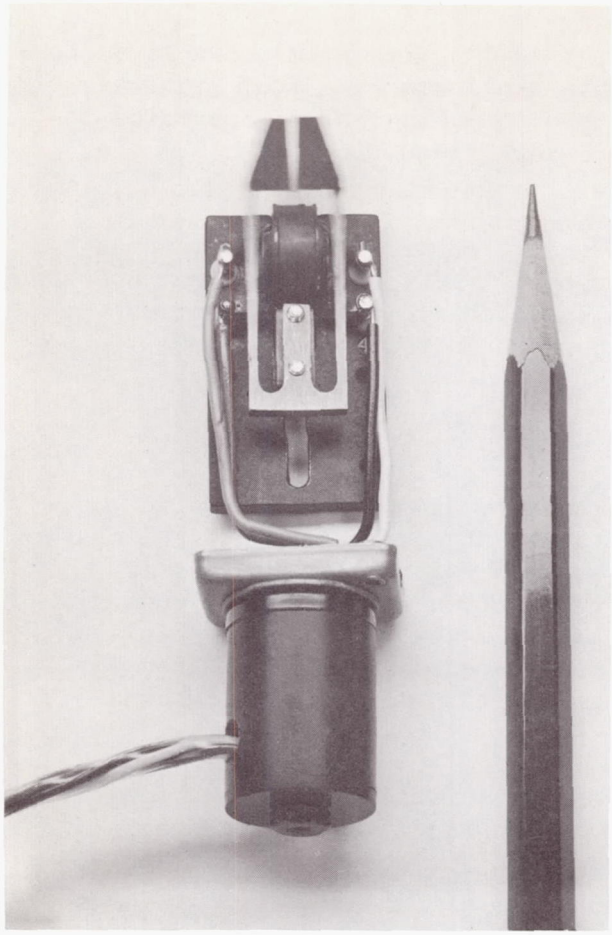

Figure 7.- Tuning fork chopper (operating).

oscilloscope. For continuous display, a rotating, interrupted wheel, as shown in figure 5, or a tuning fork chopper, shown operating in figure 7 and described in reference 27, is usually used. The radiometer output can then be displayed as a steady signal on an oscilloscope and can be compared before, during, and after irradiance (see, e.g., fig. 28).

The sources available for calibration in the ultraviolet are very weak; hence, in this regime, the radiometer output signal is sometimes too noisy (see appendix C) to be read directly on an oscilloscope. To retrieve the signal from the noise, several techniques may be employed. Simple, passive ac filtering of the modulated signal can provide improvements by decreasing the electronic band pass (see eq. (C7)), but extremely narrow band pass is not possible by this technique. Lock-in amplification (ref. 28) is used extensively for this purpose and provides a convenient means of observing signals buried in noise. A lock-in amplifier makes use not only of the frequency of the signal to be separated from the noise, but also of the electronic phase angle that this signal has with respect to a reference signal of exactly the same frequency. The reference signal is usually coupled to the chopper, either mechanically (e.g., by switches) or electronically (e.g., by coupling to the signal that drives the tuning fork). This reference signal is used to provide synchronous rectification of the desired signal, which may then be converted to a modulated dc signal. The output may be averaged then over a convenient time interval (depending on the degree of noise) to obtain effectively very narrow band-pass ac filtering of the initial signal. The result is then related via the proper constants to the peak-to-peak height of the radiometer output. Thus, signals may be detected in the presence of large amounts of noise.

Techniques of Detector Operation

Because the radiometer environment during calibration and during testing are radically different, both in time duration and intensity, it is necessary to know (1) the relationship between continuous and pulse operation and

(2) the linear operating range of the detector. The following is a discussion of (1) and (2) and of techniques for operating these detectors to ensure repeatable results.

Multiplier phototubes.- Most problems that are encountered when multiplier-phototube results are extrapolated from calibration conditions to test conditions are traceable to changes in sensitivity due to long- or short-term fatigue, or to one of several saturation phenomena. The following is a discussion of techniques that have been used at Ames Research Center to establish operating regimes and to avoid errors caused by these problems.

Multiplier-phototube fatigue depends on many operating parameters (see refs. 11 and 13). For example, sensitivity variations are usually observed when large currents are generated between the dynodes. This variation is affected by the duration of exposure to the radiation and the particular dynode voltages used. More subtly, if these voltages are changed, the variation appears to depend on the particular voltages and the duration of exposure at each voltage. For some tubes, this phenomenon has been observed even at low currents. These effects are perhaps due to alterations of the dynode surfaces by electron bombardment, or to the establishment of static charges on the support structure within the tube. Sensitivity is frequently recovered when the tube is removed from use. The extent of these effects on each tube is measured before it is put into service. For some tubes these effects are severe or the sensitivity is not recovered; such tubes are unacceptable for use in a calibrated system. At present, none of these fatigue effects is well understood, and the determination of acceptability of a given tube is an art. The present acceptance rate is about 70 percent, depending on tube type. Even after a multiplier phototube has been screened for adverse fatigue effects, there is some uncertainty in the relationship between the sensitivity of a tube that has been steadily exposed to a modulated flux, such as during calibration, and the sensitivity of a tube that has been in total darkness for a long period and then experiences a single, short-duration pulse of radiation, such as during a test event. A correction to apply to the calibration results for a possible error due to this effect is determined as follows:

It is presumed that the relationship between these two sensitivities is a constant ratio. This has been verified as reasonable in the few cases examined. To measure the effect, the conditions are adjusted so that the modulated calibration signal is strong enough to be read directly on an oscilloscope: the reading is made for the steady condition; the tube is put in total darkness for 15 to 30 minutes; then a short burst of cycles of the same modulated signal is displayed on the oscilloscope and photographed for convenient reading. The ratio of steady-state signal to short-pulse signal is the desired correction for the conditions used. In measurements made by the authors, the pulse-train length used was 0.01 sec, and the modulation frequency was 1 kHz. Tests have shown that these conditions represent well the sensitivity of very short-duration pulses such as those encountered during testing. These corrections generally are less than 20 percent and may be positive or negative.

Fatigue of multiplier phototubes has been observed when these detectors are physically attached to the facility. Apparently the shock loads from the ballistic range gun or the shock tube can damage the tube. In some instances this fatigue has been observed as a change of sensitivity over a period of months, suggesting a loss of vacuum seal of the tube envelope. Tubes are available that can withstand high accelerations and should be considered if they are to be attached to the facility without some means of shock isolation.

For convenience, the usual practice is to calibrate the radiometer at different multiplier gains so that the detector can be used for a variety of tests without being recalibrated. The gain constants in response equations (2) and (9) for a multiplier-phototube radiometer can be measured as a function of the dynode divider voltage. Figure 8 shows the result of such a determination. It is apparent from the figure that the current gain due to dynode multiplication is sensitive to variations in the divider voltage. For this reason, the high voltage is the operating parameter that must be most accurately monitored. It is routine to maintain 0.1-percent accuracy in dynode voltage.

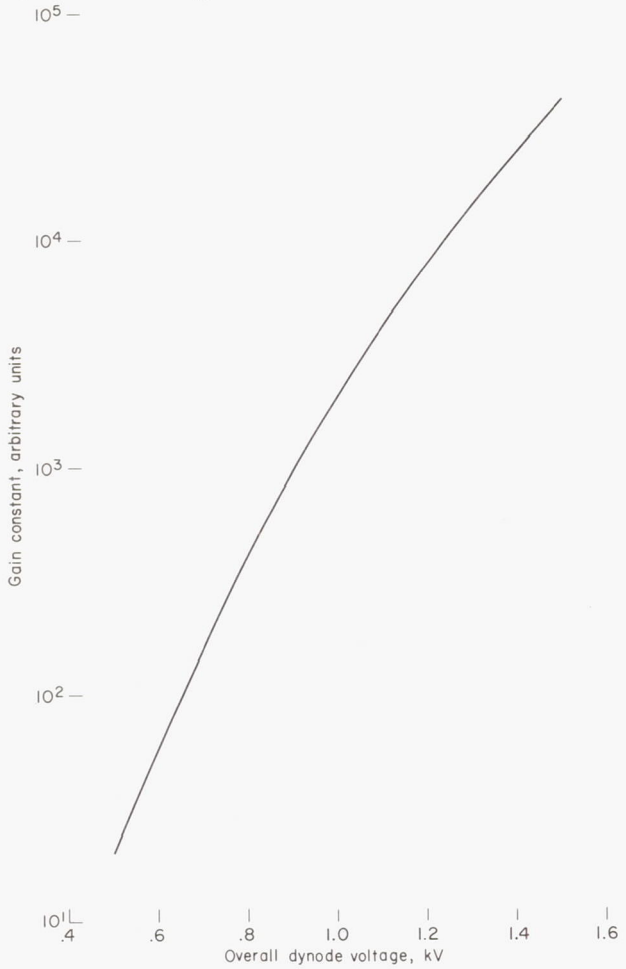

Figure 8.- Gain constant of a multiplier phototube showing variation with divider high voltage.

Multiplier phototubes are linear devices over most of their operating range when used in the manner discussed; doubling the incident flux doubles the output current. The upper limit of this linear range is determined by one of several saturation phenomena. Apparently there is no lower limit; linearity is retained with signals so weak as to be barely detectable from the inherent noise.

The saturation phenomena that limit linearity are: (1) photocathode saturation resulting from excessive cathode current; (b) space charge effects due to alteration of the static field between dynodes by the presence of the current electrons; (c) dynode voltage divider saturation, resulting from high currents within the tube, which are drawn from the divider and which cause a voltage change therein; and (d) saturation of the subsequent electronic system (i.e., close-coupled amplifier or oscilloscope). If a fixed cathode area is irradiated, it is not necessary to differentiate between the first two phenomena mentioned. However, in the case of the monochromator-radiometer, the cathode

area varies (because of the variable exit slit width and the divergence of the exiting beam). The effect of this will be discussed later. Divider capacitors are used to present the long-duration (msec) calibration pulses from changing the dynode voltages, which would result in voltage-divider saturation. During short test events (μsec), the charge depletion of these capacitors is so small that space-charge effects limit the linear operation at dynode currents much lower than those that would cause divider saturation. It should be noted that extraneous radiation falling on the photocathode loads the radiometer and promotes saturation during pulse response.

The method of determining saturation is exactly as described in reference 2. A filter is measured for apparent transmission by placing it in and out of a radiation beam incident on the radiometer. The ratio of the readings is the transmission if the radiometer is operating linearily. If the transmission is repeatedly measured with increasing radiation intensity, eventually the radiometer with the filter out of the beam will be slightly saturated. This is noted by an increase in apparent transmission. The upper limit to the linear operating range of the radiometer is thus determined. Saturation effects are dependent on pulse lengths when divider capacitors are used (see appendix B), so the radiation source should have approximately the same time duration as the test source. For ballistic-range applications, pulsed gas discharge tubes with a duration of about 2 μsec may be for evaluating saturation effects.

The measured limit of the linear behavior of a multiplier phototube is shown in figure 9. The output voltages were measured at the multiplier-phototube anode and were plotted as equivalent output from the amplifier described in appendix B (see fig. 23). In figure 9, the maximum output voltage for linear operation is plotted as a function of the overall dynode divider voltage. The maximum linear amplifier output is shown as a constant value - nominally, 5 V.

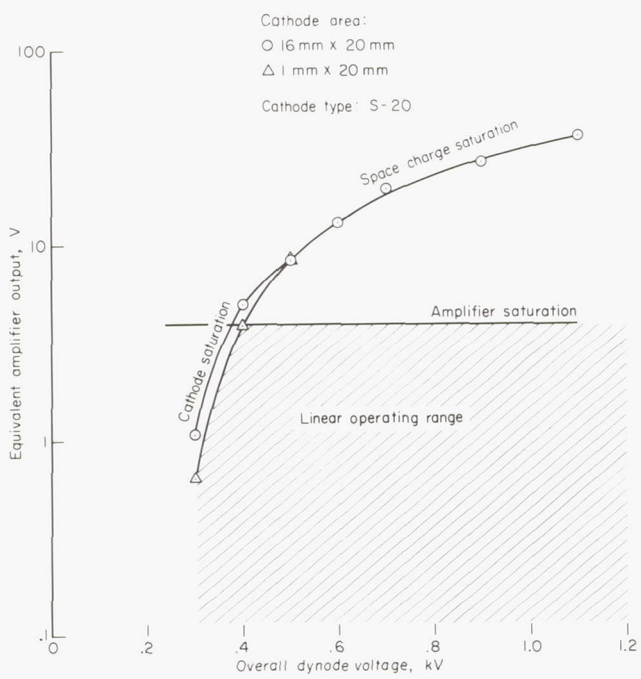

Figure 9.- Multiplier phototube and amplifier saturation.

The saturation of the multiplier phototube at divider voltages greater than about 600 V was from space-charge saturation alone. Cathode saturation effects are noted at lower divider voltages.

The larger irradiated cathode area (6 mm by 10 mm) corresponds approximately to the maximum attainable when the multiplier phototube is used with the described monochromator (see fig. 17). The area was reduced to 1 mm by 10 mm to correspond to a narrow exit slit setting. The difference in the resulting curves indicates that in this range a

contribution to the saturation was produced by cathode saturation. Manufacturers' data for multiplier phototubes usually include the maximum cathode current that is linearly related to irradiance. Calibrated neutral filters may be required to prevent the phototubes from exceeding this current.

If only a termination resistor were used (no amplifier), the proper operating range would be below the curve, corrected to account for amplifier gain. The hashed area in figure 23 indicates the proper operating range for the amplifier shown. Note that if the divider voltage is above 400 V, the amplifier saturates at a voltage that still allows the multiplier phototube to operate linearly. This saturation has a recognizable characteristic; it results from clipping of the waveform by the output stage of the amplifier so that it is easy to ascertain from the oscillogram of the test whether the instrumentation was saturated. This is not the case with the other mentioned causes of saturation, as the waveform is not recognizably altered. At lower divider voltages, the space-charge effects or cathode saturation determine the maximum linear output voltages.

Solid-state infrared detectors.- As noted previously, the mechanism of photocurrent generation in these detectors is somewhat different from that in multiplier phototubes; consequently, different procedures must be considered. In particular, the linearity and rise time of the detector is strongly influenced by the circuit in which it is incorporated; hence, it is important to measure these parameters with the exact circuit that will be used during testing.

As mentioned in a previous section, maintaining low voltage across the detector terminals produces linear operation. The reason for this behavior is seen in figure 10. Shown here is the dc equivalent diode circuit used in reference 29, connected to an external circuit that presents the detector with load, R_E. The diode is assumed to consist of a current generator with output, i_ϕ, proportional to the irradiance, paralleled by a diode and a leakage resistance. Note that the internal voltage gradient of the diode junction causes current to flow in the forward direction of the diode (ref. 14), and hence must have a polarity opposite to the diode current, i_D, and the leakage current, i_L. A summation of the currents at a junction shows that $i_E = -i_\phi + i_D + i_L$. The diode current is given by reference 29 as an equation of the form

$$i_D = i_S[\exp(Bv) - 1]$$

where i_S and B are characteristics of the particular diode, and v is the voltage across the diode. The leakage current is v/R_L, so that the external current may be written:

$$i_E = -i_\phi + i_S[\exp(Bv) - 1] + \frac{v}{R_L} \quad (19)$$

Clearly, as v approaches zero, the second and third right-side terms of

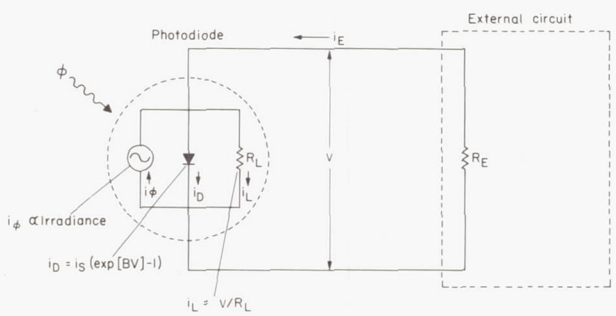

Figure 10.- Equivalent circuit for photodiode.

equation (19) vanish, and the external current is in proportion to the photon-induced current. Obviously, one method for making v approximate zero is to make R_E as small as possible, since $v = i_E R_E$. The extent to which v can become nonzero and not induce appreciable nonlinearity depends on the diode parameters of the individual detector. The diode parameters are obtained by fitting the above equation to a determination of i as a function of v for a condition of constant irradiance. This is done simply by impressing a series of voltages across the detector and observing the resultant current. Figure 11 is a measured current-voltage curve for a cooled InSb detector; the circuit used for the measured is also shown in the figure. The least squared-error fit of equation (19) to this curve gave the following diode parameters:

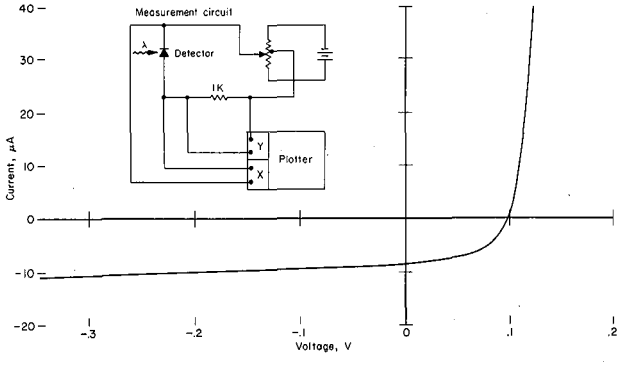

Figure 11.- Diode curve for cooled (77° K) InSb infrared detector.

$$i_S = 1.723\times10^{-9}\ \text{A}$$

$$R_L = 1.75\times10^{5}\ \Omega$$

$$B = 86.5559\ \text{V}^{-1}$$

Substituting these values in equation (19), one can obtain the detector current at which the output is 10-percent nonlinear (i.e., $i/i_\phi = 0.9$) as a function of detector load impedance. Figure 12 illustrates the results of this calculation for the detector mentioned above; shown also as $\bar{i}_b$ in the figure is the current induced by the 297° K background. Note that for impedances greater than 100 ohms, the effective dynamic range of the detector becomes severely restricted.

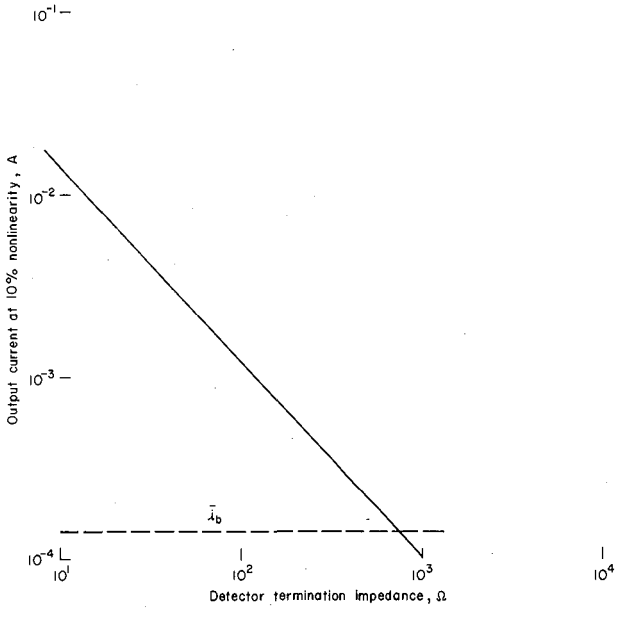

Figure 12.- Nonlinearity limits for InSb detector.

Clearly, the nonlinearity limits for a given detector will be a strong function of its diode parameters, particularly the saturation current, i_S. Hence, if the detector is to be terminated by more than a few tens of ohms, it would be prudent to ascertain linearity limits, either by measurement of diode parameters or by direct measurement of the signal output as a function of irradiance.

Absolute calibration of these detectors is done as has already been discussed, by utilizing a heated cavity as the radiation standard. The source strengths available are

usually adequate to measure the sensitivity at a series of intensities to cover the desired range of test intensities. Of the detectors examined, those that used the low-impedance amplifier described in appendix B, exhibited linear behavior over the entire operating range of the radiometer, from signals just discernible from the amplifier and background shot noise (the limiting noise sources), to signals just saturating the amplifier - a dynamic range of about 3 decades.

Rise time is a function of the particular detector and of conditions imposed by the subsequent amplifier, and it is not readily calculable. It has been observed by the authors that the rise time of an InSb detector is affected by the bias voltage and is near a minimum at zero volts. For short-event applications, the reduction of infrared data often requires accurate knowledge of rise time and fall time. Thus, it is advisable to measure these properties directly. There are several types of solid-state infrared radiation sources that are suitable for this purpose. The authors have used a commercially available GaAs light-emitting diode (HP Associates model 4106) that emits radiation when a current pulse is applied. The spectral emission from this diode is a strong band at 0.9 μ and a weak continuum extending to about 1.5 μ. The time response of the 0.9-μ band radiation was measured as follows.

The diode was set up to irradiate an S-1 type multiplier phototube through a filter that isolated the radiation at 0.9 μ. A short rise- and fall-time rectangular current pulse was applied, and the output of the multiplier phototube noted. The diode emission was observed to follow the current pulse to within 40 nsec, which was the readout system time response. This source was then used to measure the time response of a cooled InSb infrared detector at 0.9 μ. Figure 13 shows an oscillogram taken during this measurement. The irradiance was too weak to obtain a noise-free signal from a single pulse, so a large number of sweeps were averaged. The upper trace shows a single sweep superimposed on the record of many sweeps. The lower trace is from the current pulse through the diode (representing the radiation pulse shape). The rise time observed in this case is shorter than 0.5 μsec, indicating that these detectors can be used to time-resolve infrared events to this time scale without having to make large corrections to the data to account for detector time response. This agrees with the response times given for cooled InSb given in reference 7.

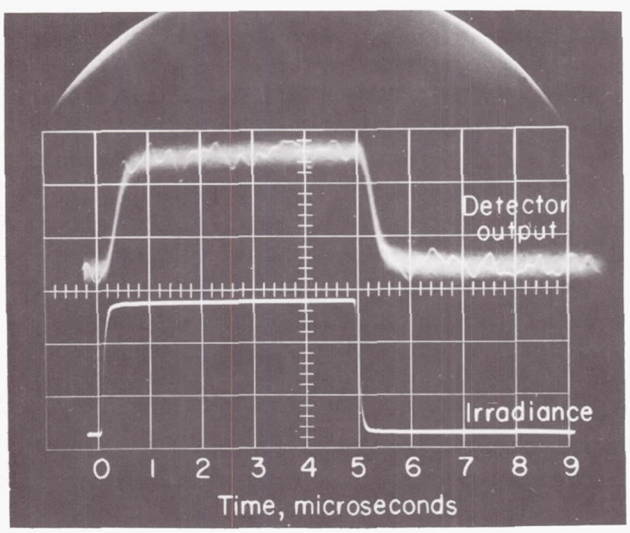

Figure 13.- Oscillogram showing rise time of InSb radiometer.

When making measurements such as described above, it is important to filter the output from this emitting diode to exclude the long wavelength continuum. If this portion of the radiation is included in the

irradiance to the infrared detector, a much longer time response is observed. This is apparently due to slow time response of the long wavelength portion of the diode radiance rather than to the detector rise time being wavelength dependent. To verify this a liquid nitrogen cooled InAs emitting diode (Texas Instrument) was used to make the same measurement. The manufacturer's specifications for this diode indicate that the spectral radiant output is confined to wavelengths between 1 and 3.3 μ, and that the rise time is about 100 nsec. This device is spectrally better suited than is the GaAs emitting diode for measuring the rise time being described. However, the InAs diode is mounted in the bottom of a small Dewar, much like the cooled IR detector, and it is optically much more difficult to couple this source to the detector. The detector rise time observed with this source was essentially the same as that obtained with the GaAs source.

The preceding results are for cooled InSb detectors. Doped semiconductor materials for use at longer wavelengths may show dual time constants; that is, response at short wavelengths may differ from response at long wavelengths (ref. 7). Additionally, rise time and fall time may be different.

The various mechanisms that cause drift in multiplier phototubes have no obvious counterparts in solid-state detectors. Solid-state detectors should have good long-term stability of sensitivity. Stability of sensitivity of solid-state detectors has not been investigated extensively by the authors; however, the following test was made.

A commercially available, cooled InSb detector was set up and the response to a 500° K blackbody source was measured several times a day for five days. It was found that the variation over an 8-hour period was less than 0.5 percent, and the variation from day to day was on the order of 1 percent. It is believed that this level of stability is typical of a detector in good working order.

APPLICATIONS

The preceding discussion has been confined to that of individual radiometers, but seldom is a single radiometer sufficient for experimental apparatus. Instead, complicated arrangements usually result from design to a particular application. It is, therefore, of interest to consider radiometer systems that are actual data collection systems. Three diverse systems currently in use at the Ames Research Center will be discussed.

The first system consists of three monochromator-radiometers arranged in such a way as to have a common optical axis normal to the flow within a shock tube (fig. 14). The radiation in a direction along the optical axis from the hot gas contained in the view field is diverted to the radiometers via the partially transmitting mirrors. This system was used by Arnold (ref. 8) to study chemical kinetics.

A second system consists of a grating monochromator (with four gratings) whose effective entrance slit is the radiating shock layer of a blunt

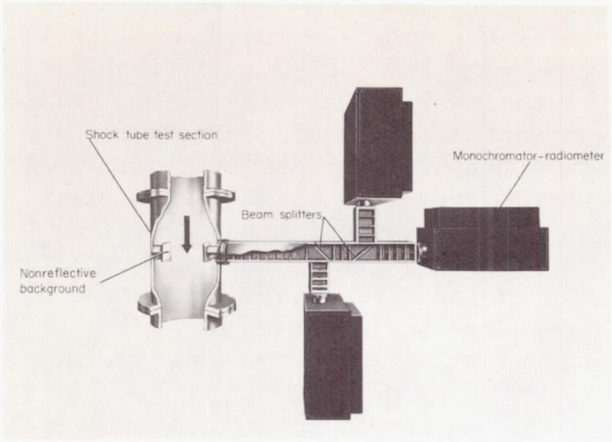

Figure 14.- Shock tube radiometer system using three monochromator-radiometers with a common optical axis.

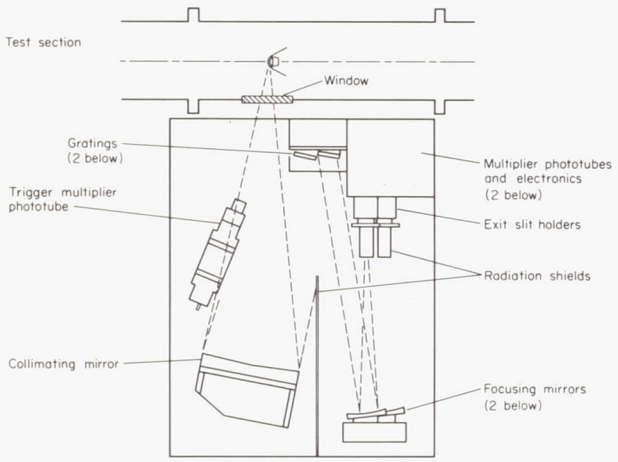

Figure 15.- Schematism of 4-channel scanning monochromator.

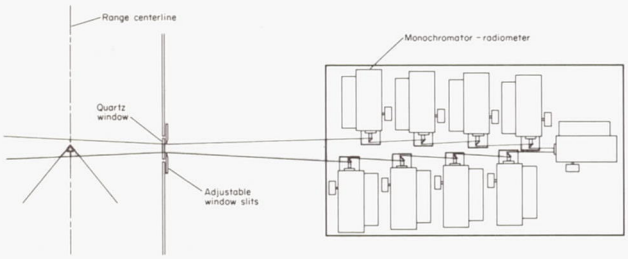

Figure 16.- Schematism of multichannel radiometer upper bank drawn to scale.

ballistic-range model, and which has four exit slits, each equipped with a multiplier phototube (fig. 15). Ideally, the ballistic-range model should be blunt and should exhibit only bow-shock radiation; this system could then be employed to give continuous coverage over a wide spectral range at the sacrifice of spatial resolution of the radiation. The gratings are adjusted so that each detector receives a different spectral range, thus providing total coverage from 0.2 to 1.0 μ with no interference from higher orders of the gratings (see page 6). This instrument is described in detail in reference 30. The four-channel instrument is an extension of the single-channel scanning monochromator described in reference 31. The earliest reference to such a device appears to be reference 32.

A third system, which has not been described elsewhere, is a multichannel radiometer consisting of 18 monochromator-radiometers. This system is used primarily to study radiation spatially resolved in the direction of travel from the flow fields of ballistic models. The radiometer system is on two tables, one of which is shown schematically in figure 16 (drawn to scale). Each table forms a base for nine channels. A channel consists of an individual monochromator-radiometer equipped with a multiplier phototube (fig. 24) and a mirror, and is shown in figure 17. Incoming radiation is directed by mirrors into the entrance slits. The model travels only a short distance during the period of data collection; thus each mirror can be adjusted so that the optical path within the monochromator remains fixed for both calibration and experiment. Each monochromator is a Bausch and Lomb instrument of 25-cm focal length, having all internal optics

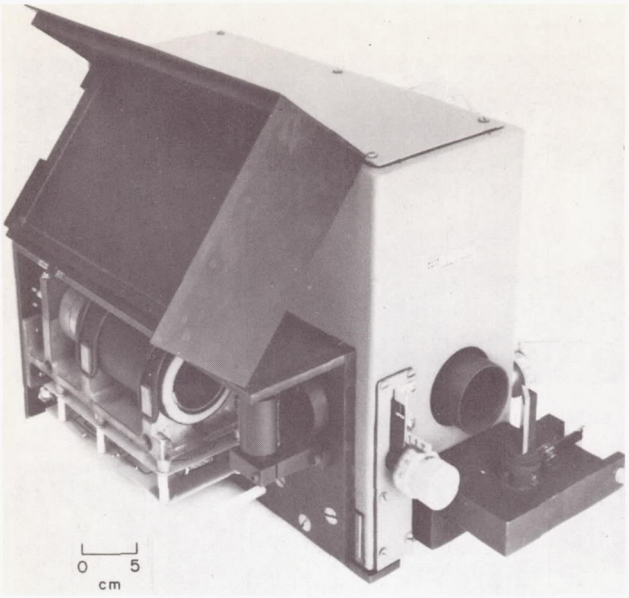

Figure 17.- Monochromator-radiometer as used in the 18-channel radiometer.

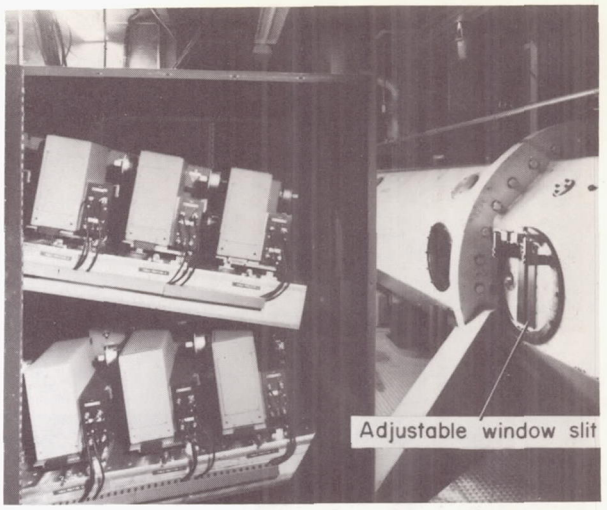

Figure 18.- 18-channel radiometer system before the Ames Hypersonic Free-Flight Radiation Facility.

reflective; it allows spectral resolution from a few angstroms to 800 Å, using a 600-line/mm grating. The entrance and exit slits are independently adjustable. Each channel observes the model in the view field with an optical direction not exceeding a few degrees from a normal to the flight path. The second table is located beneath the top table, in an identical position, except that the optical path is displaced in rotation from the top table 17.5° about the flight path. This angle was shown to introduce negligible error for cone models flying at angle of attack, based on results reported in reference 33. In figure 18, the front half of the entire radiometer system is shown positioned before the Ames Hypersonic Free-Flight Radiation Facility. The entire system assembly can be moved without disturbing any of the component radiometers. Recording oscilloscopes and power supplies are located remotely, and all electrical connections are made at the panel at the rear of the assembly.

Final alinement for each radiometer channel is by means of mounts that allow translation within the frame. A point light source is moved about on the center line of the test section in the view field, and the channels are adjusted so that each mirror (figs. 16 and 17) is as close to the center of the table as possible without eclipsing the other mirrors farther from the test section. This arrangement minimizes the total horizontal angle subtended by the outermost mirrors. The mirrors are then adjusted so that the beam is centered on the entrance slit.

The slit at the test-section window is adjustable from fully closed to 5 cm to provide a range of view-field widths within the test section. The penumbra of the view field is controlled by the monochromator entrance slit width, and thus may be vanishingly small compared with the view-field width. A typical oscillogram obtained from a channel during the ballistic-range test of an ablating plastic model is shown in figure 19. The settings for the

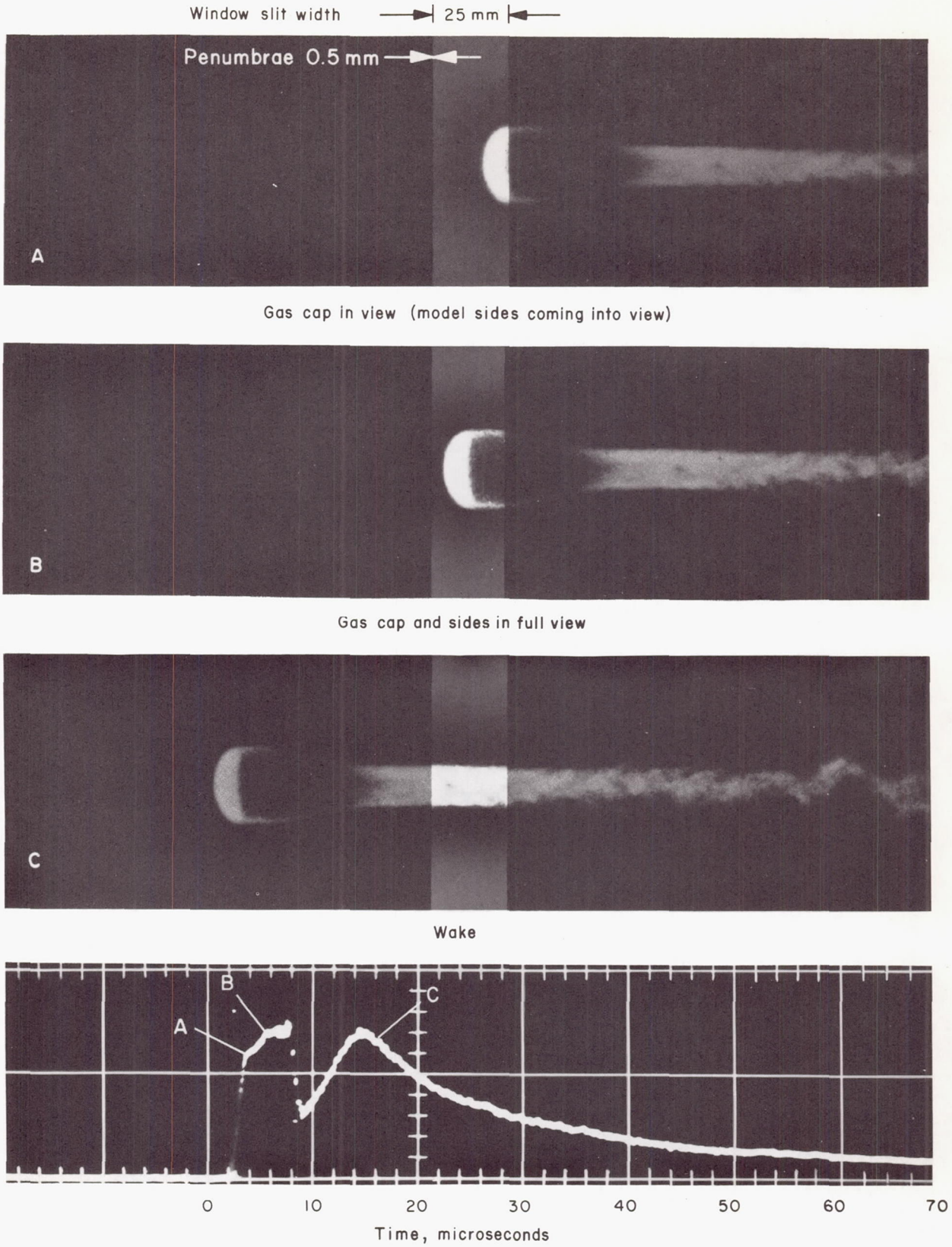

Figure 19.- Oscillogram obtained from ballistic range test with a multiplier-phototube radiometer.

channel were: entrance slit, 0.5 mm; exit slit, 8 mm; and distance from flight path, 1 m. Features of this oscillogram are indicated and matched with pictures of the model placed in proper position with respect to the radiometer view field. The radiating flow field around the model and in the wake are clearly visible. Note the change in slope of the trace when the sides of the model have come fully into the view field. The rapid change of the radiometer output as the model enters and leaves the view field indicates the narrow penumbra (0.5 mm) and short rise time of the radiometer (approximately 40 nsec). It is instructive to compare this figure with the corresponding figure of reference 2 obtained under similar conditions, but with much wider penumbra and a longer rise-time radiometer. With various combinations of multiplier-phototube types and monochromator grating blaze angles, the system can in practice contiguously cover the spectral region from 0.2 to 1.1 μ with good sensitivity.

Ames Research Center
National Aeronautics and Space Administration
Moffett Field, Calif., 94035, June 27, 1969

APPENDIX A

MATHEMATICAL MODEL OF MONOCHROMATOR-RADIOMETER RESPONSE

A radiometer, as discussed in this paper, consists mainly of a quantum detector, a spectral filter, and an amplifier, and has some means of defining the view field. The spectral filter may be any of several devices; in this appendix a grating monochromator will be considered for use as the spectral filter.

A monochromator used as the filter has the desirable feature of being variable in spectral coverage and band-pass shape. However, for convenient use of the radiometer, it is desirable that the absolute spectral sensitivity be controllable and describable in terms of calibration constants. Before a radiometer can be calibrated and used as a variable wavelength and band-pass-shape instrument, equations must be derived that define its performance in terms of the controllable parameters (viz., wavelength setting and slit widths). These equations indicate the most efficient calibration procedure and predict absolute spectral sensitivity under a variety of conditions.

In this appendix a response equation will be derived. The derivation relies on a derived normalized monochromator transfer function that will also be discussed and compared with measured results.

RESPONSE EQUATION

Grating Monochromator

The response of a monochromator-radiometer to a radiation source is, in general,

$$v = G \int_0^\infty \Re(s_1, s_2, \lambda_o, \lambda) H(\lambda)\, d\lambda \qquad \text{(A1)}$$

where

v	radiometer output, V
G	electronic sensitivity, $(V)_{output}/(A)_{detector}$
$H(\lambda)$	spectral irradiance from the source, $W/cm^2\text{-}\mu$
$\Re(s_1, s_2, \lambda_o, \lambda)$	spectral response of the radiometer, here considered to be additionally a function of the monochromator slit widths and grating drive setting, $(A)_{detector}/(W/cm^2)_{incident}$

s_1, s_2 entrance and exit slit widths, respectively, cm

λ_o monochromator grating drive setting, μ

λ integration variable representing wavelength, μ

When a multiplier phototube is used for the detector, we will define the detector current as the cathode current and associate the resultant dynode multiplication with the system electronic sensitivity, G.

The spectral response of the radiometer, $\Re$, is derived as follows. The spectral power, P_2, at the exit slit plane, contained in a monochromatic image of the entrance slit, is given by:

$$P_2(\lambda) = s_1 \ell H(\lambda) \tau(\lambda), \ W/\mu \tag{A2}$$

where $\tau(\lambda)$ is the aggregate transmission of the internal components of the monochromator, and ℓ is the height of the entrance slit, cm. The normalized transfer function, $f(\lambda)$, is the geometric fraction of the monochromatic entrance slit image passing through the exit slit, normalized to unity.[1] The fraction, $f(\lambda)$, of this power that leaves the exit slit is:

$$f(\lambda) = \begin{cases} f(\lambda) & \text{for } s_1 \leq s_2 \\ \left(\frac{s_2}{s_1}\right) f(\lambda) & \text{for } s_1 > s_2 \end{cases} \tag{A3}$$

for an equal focal length camera and collimating optics (i.e., the entrance slit magnification is unity). It is seen in figure 20 that the maximum fraction of the entrance slit image leaving the exit slit is unity, or s_2/s_1 for the two cases indicated by equation (A3). Assuming that all the radiation that leaves the exit slit arrives at the sensitive area of the detector, we can rewrite equation (A2), using equation (A3), and we have the power at the detector,

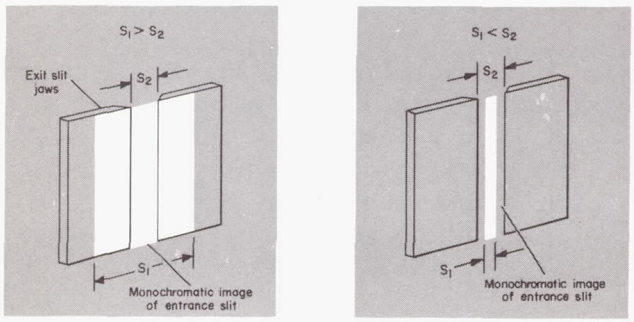

Figure 20.- Sketch showing relation of exit slit and entrance slit monochromatic image (at $\lambda = \lambda_o$) for $s_1 > s_2$ and $s_1 < s_2$.

$$P_o = P_2 f(\lambda) = \ell \, MIN(s_1, s_2) \tau(\lambda) f(\lambda) H(\lambda) \tag{A4}$$

where $MIN(s_1, s_2)$ is equal to the smaller of the arguments. Finally,

[1]For the case of a filter radiometer, the analogous normalized transfer function is simply the normalized filter transmission.

if the quantum efficiency of the detector is $\mathcal{E}(\lambda)$, the spectral response of the radiometer is given by

$$\mathcal{R} = \frac{P_o \mathcal{E}(\lambda)}{H(\lambda)} = \mathcal{l}\,\mathrm{MIN}(s_1, s_2)\,\tau(\lambda)\mathcal{E}(\lambda)f(\lambda) \tag{A5}$$

If $\mathcal{l}$ is taken to be a constant, the response equation, (A1), becomes

$$v = \mathcal{H}\,\mathrm{MIN}(s_1, s_2) \int_0^\infty F(\lambda) f(\lambda) H(\lambda)\, d\lambda \tag{A6}$$

where $\mathcal{H} F(\lambda) = G\mathcal{E}(\lambda)\tau(\lambda)\mathcal{l}$.

Under this definition, $\mathcal{H}$ is not taken to be a function of λ; hence, the wavelength dependent terms are contained in $F(\lambda)$. To evaluate the functions $\mathcal{H}$ and $F(\lambda)$ separately, we define for convenience:

$$F(\lambda) = \frac{\tau(\lambda)\mathcal{E}(\lambda)}{[\tau(\lambda)\mathcal{E}(\lambda)]_{MAX}} \tag{A7}$$

whereby then

$$\mathcal{H} = G\mathcal{l}[\tau(\lambda)\mathcal{E}(\lambda)]_{MAX} \tag{A8}$$

Note that $[\tau(\lambda)\mathcal{E}(\lambda)]_{MAX}$ is a constant, and $F(\lambda)$ has a maximum value of unity according to this definition. Variations in sensitivity of the radiometer that are caused by changes in the system current gain (e.g., changes in multiplier-phototube high voltage) are manifest in $\mathcal{H}$, and variations caused by changes in spectral coverage of the radiometer (viz., change of grating position within the monochromator) are manifest in $F(\lambda)$. Calibration of the monochromator-radiometer consists in determining the functions $\mathcal{H}$ and $F(\lambda)$; as discussed in the text of this report.

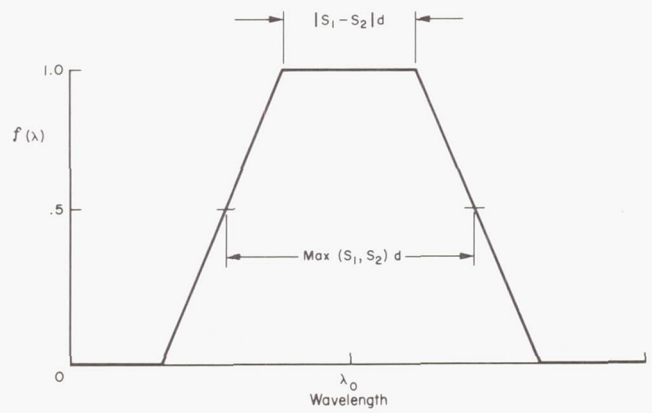

Figure 21.- Analytic form of normalized transfer function of a monochromator-radiometer.

The normalized transfer function $f(\lambda)$ is shown in figure 21 for slits wide enough that the diffraction image size may be neglected; grating orders above the first order are assumed to be blocked. The half-width (width of the trapezoid at $f(\lambda) = 1/2$) is given by the function $\mathrm{MAX}(s_1, s_2)$, which is equal to the larger of the arguments, multiplied by the monochromator reciprocal dispersion d, in μ/cm. The width of the flat portion at $f(\lambda) = 1.0$ is given by the indicated formula, which reduces the transfer function

to the familiar triangular shape when the slit widths are equal. The reader is directed to reference 34, chapter 6, for a derivation of the above figure that shows the normalized transfer function.

The following is an empirical determination of $f(\lambda)$ for a monochromator-radiometer. This determination consists in showing experimentally that the form given in figure 21 is indeed applicable to the instrument. This will be done in two parts: first, it will be shown that the output signal of the radiometer obeys the response equation that is obtained when the form of $f(\lambda)$ is used in the equation; and, second, it will be shown that the functional shape of $f(\lambda)$, measured at the selected wavelength and slit widths, is the same as shown in figure 21.

A continuum source is convenient for performing the first test. Equation (12) is applicable for this case:

$$v = \iint F(\lambda_o) H(\lambda_o) s_1 s_2 d \tag{A9}$$

where $H(\lambda_o)$ is the spectral irradiance from an arbitrary continuum source. Thus, if a matrix of radiometer output voltages is compiled as a function of the slit widths, s_1 and s_2, with all other parameters in the above equation fixed, and it is found that the voltage is proportional to their product, then it may be assumed for this case that the radiometer is obeying the response equation.

In a radiometer design developed by the authors that utilized eighteen 25 cm focal-length monochromators, each with a reciprocal dispersion of 0.067 μ/cm, it was found that the radiometer followed the above proportionality if an effective slit width was used. This is defined as follows:

$$s = \mathcal{s} - \delta \tag{A10}$$

where $\mathcal{s}$ is the indicated slit width, and δ is an offset correction that is determined empirically for each slit drive by measuring the radiometer output over a range of signals and choosing the value of δ that best fits the response equation to the data. The method of determining effective slit widths gave acceptable agreement between predicted and measured radiometer outputs over a range of slit widths from 0.05 cm to 1.0 cm. The offset corrections were from 0 to 0.02 cm for this system. In the initial adjustment of the slit drives, the slit jaws were closed and the knob was set on the shaft to indicate 0; thus, the "offset" corrections discussed here do not represent a simple mechanical offset.

The form of $f(\lambda)$ could be obtained by irradiating the entrance slit of the monochromator-radiometer with a monochromatic beam of variable wavelength. As the wavelength of the incident beam is varied in the region about λ_o, the output of the radiometer will be proportional to the instantaneous value of $f(\lambda)$, assuming that the power in the beam remains constant (see eq. (17)).

Since it is sometimes difficult to obtain a monochromatic beam that meets the above requirements and whose power is independent of wavelength, an alternate approach employs an isolated atomic line for a source (e.g., a line from a low-pressure mercury lamp). Varying λ_o in the vicinity of the line has the effect of causing the function $f(\lambda)$ to scan across the line wavelength; the corresponding output is proportional to $f(\lambda)$ as defined on the slit settings being used.

Figure 22 shows the functions $f(\lambda)$ as determined for two slit settings on a 25-cm focal-length monochromator-radiometer. The points represent the data, and the dashed lines represent the given form for $f(\lambda)$. The agreement between data and given form is excellent here, as it is in many other combinations of slit widths from several monochromators examined by the authors. However, when slit widths of 0.05 cm or less are considered, the data and theory begin to diverge. This lack of agreement might be due in part to the manner in which slit width is determined, namely, $s = s - \delta$. The offset is determined by assuming that the energy leaving the slit and arriving at the detector is proportional to the slit-reading less the offset. If the slit jaws are not parallel, or if the drive is not accurate, then the actual zero width cannot be determined by extrapolation in the manner defined.

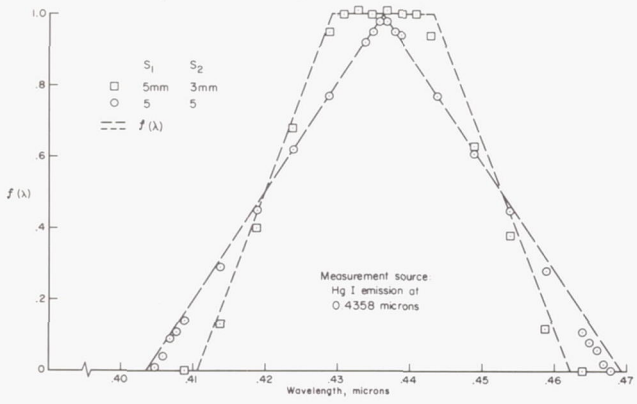

Figure 22.- Comparison of measured and analytical transfer function.

It is evident that for precise narrow band-pass radiometry, such as isolation of one particular sequence of a molecular system, the center wavelength and spectral band-pass shape of the monochromator-radiometer must be accurately known. Small error in knowledge of λ_o might lead to severe attenuation in the spectral region of interest. It is possible to perform the calibration by determining $f(\lambda)$, as has been outlined, using a line as spectrally near the region of interest as possible. This provides a wavelength drive calibration that can be transferred to the required setting, as well as spectral band-pass calibration. Reference 8 discusses work of this nature, and the calibration procedures are discussed therein.

Prism Monochromator

The preceding analysis of the behavior of a detector fitted to a grating monochromator applies to the use of a prism monochromator if the user accounts for the nonlinear dispersion of the prism. The normalized transfer function for a prism monochromator is not constant with λ_o (as it is for a grating monochromator used near normal incidence). The transfer function usually increases in half-width with decreasing wavelength (depending on prism material and wavelength). Reference 35 gives results of measurements of prism monochromator transfer functions that would be useful in this instance.

APPENDIX B

AUXILIARY ELECTRONICS FOR MULTIPLIER PHOTOTUBES AND SOLID-STATE INFRARED DETECTORS

By Donald E. Humphry

In general, the detectors described in this paper are not capable of driving recording equipment (e.g., oscilloscopes) directly. For short rise-time use, multiplier phototubes and the InSb infrared detectors require matching of their impedances to those of the cables connecting them to the recorders; also each requires its own particular support electronics. The multiplier phototube requires a voltage divider to supply an array of voltages to the dynodes in order to achieve electron multiplication. Capacitors are required at the dynodes to maintain these voltages during high-level pulses when the currents within the tube cease to be negligible compared to the divider current. The infrared detector requires a means of controlling the bias voltage it generates from the ambient radiation flux. In addition, the infrared detector exhibits improved performance if it is used with a low impedance circuit.

MULTIPLIER PHOTOTUBES

A multiplier phototube may be operated with the anode terminated by a noninductive resistor; but to drive a remote oscilloscope, the low resistance required for high-frequency response results in low voltage signals. These signals must be made high enough (by amplification within the tube) to dominate subsequent recorder system noise, including noise externally induced into the cable. Amplifying the current within the tube in order to overcome recorder system noise reduces the dynamic range of the system. A large improvement is realized if a high-frequency response amplifier is closely coupled to the detector. Close-coupling reduces the externally induced noise into the lead from the multiplier phototube to the amplifier and reduces the capacitance at the amplifier imput. A larger resistance may then be used to achieve the same frequency response which results in a desirable voltage increase at this point. The signal is then amplified and the amplifier terminated with the correct cable impedance.

The dynode voltage divider is comprised of a series of resistors through which a current is passed. The dynodes are connected to these resistors to obtain the necessary voltages. Reference 12 contains a general discussion of multiplier-phototube voltage dividers. Here we are concerned with optimizing the dynamic range for pulse operation. Electron multiplication is very sensitive to any changes in dynode voltages, so it is necessary to keep these voltages constant despite the relatively long duration pulses that are produced during calibration. This is achieved by bypassing the dynode divider

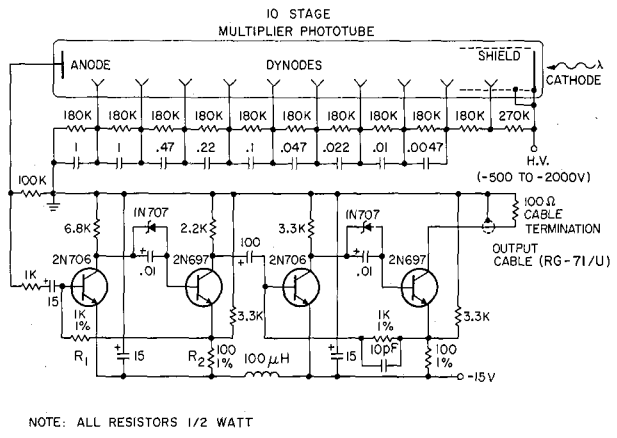

NOTE: ALL RESISTORS 1/2 WATT

Figure 23.- Multiplier-phototube amplifier and dynode voltage divider.

resistors to ground with a series of capacitors, see figure 23. The size of the capacitors required depends on the magnitude and duration of the current pulse within the tube and the resistance of the dynode voltage divider. The capacitors were chosen to maintain the dynode voltages within 10-percent for an arbitrary adverse operating condition; namely, low over-all dynode divider voltage, high cathode current, and long-duration pulse length. The values were: 50 V per stage, 20 μA, and 0.001 second. The least current is drawn from the cathode to the first dynode and becomes more to each dynode, progressing toward the anode. Thus the last dynode requires the largest capacitance, with each preceding dynode requiring progressively less. The first dynode is not bypassed because here the current within the tube is always negligible compared to the dynode divider current. A dynode voltage divider with capacitors is shown as part of the amplifier circuit in figure 23.

If the output of the multiplier phototube is used directly without an amplifier, the rise time depends on the value of the output resistor and the amount of capacitance in parallel with it (usually from the cable and the oscilloscope input capacitance). The rise time, τ_r, is approximately twice the time constant, that is, $\tau_r \cong 2RC$, where R and C are the above-mentioned resistance and capacitance. However, if a coaxial cable is properly terminated by a resistance equal to its characteristic impedance, the cable does not contribute to the above capacitance.

The amplifier in figure 23 is a current amplifier with a gain of 121. It is in two stages, each having a current gain of 11. Each stage is composed of two transistors with feedback such that the current gain is controlled by the ratio of two resistors, and is given by $[1 + (R_1/R_2)]$. The gain, then, is practically independent of transistor parameters and can be changed easily by varying the feedback resistor ratio. The output of the amplifier is connected to an oscilloscope by means of a coaxial cable (RG-71/u), and terminated at the oscilloscope with its characteristic impedance (100 Ω is used for convenience instead of 93 Ω, which is exact for this cable). This is necessary in order to avoid distorting the leading edge of a fast-rising pulse.

The amplifier is designed to operate with a negative input pulse (viz., output of a multiplier phototube), and it is with this type of an input that it has the greatest dynamic range, approximately 5 V into 100 Ω. Care must be taken when the multiplier phototube is receiving a steadily modulated radiation signal, such as a square wave as is produced during radiometer calibration, because the amplifier saturates on a positive signal at about 0.2 V. This saturation is not apparent from the observed wave shape. With this type

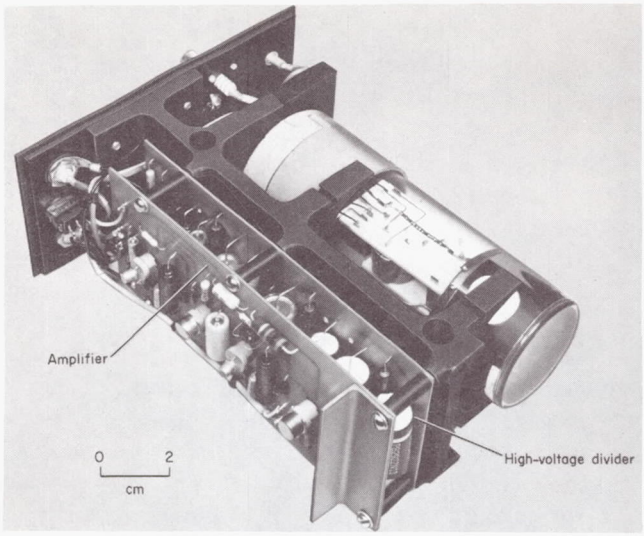

Figure 24.- Multiplier-phototube assembly, including dynode voltage divider and amplifier.

of signal input, the output should be limited to 0.4 V, peak-to-peak. The band pass of the amplifier is from 5 Hz to 8 MHz at the 3 DB points.

Figure 24 is a photograph of this amplifier, including a voltage divider, multiplier phototube, and integral mounting frame.

When the amplifier described above is used, the level of output noise is normally determined by the noise in the multiplier phototube itself (see appendix C). The amplifier-generated noise is approximately 10 mV and is negligible if the multiplier phototube is operated at high gain.

SOLID-STATE INFRARED DETECTORS

The amplifier used with the InSb infrared detector is shown schematically in figure 25. The amplifier is a current amplifier with a total current gain of 1300 and a band pass from 5 Hz to 1 MHz. The input impedance is approximately 10 Ω. The output of the amplifier drives a cable terminated with 100 Ω.

Since this amplifier has high gain and a wide-frequency response band, there is a problem of undesirable feedback that results in an oscillation of the amplifier. Therefore, the amplifier and the detector are mounted in the same chassis with minimum lead length between the detector and the output of the amplifier and with component placement that minimizes the likelihood of this undesirable feedback. In addition, a mechanical baffle is used to separate the input stage of the amplifier from the detector. This is done to avoid a possible zero shift between the input stages due to the cooling effect of the cold detector environment. Two complete amplifier and detector assemblies are shown in figure 26.

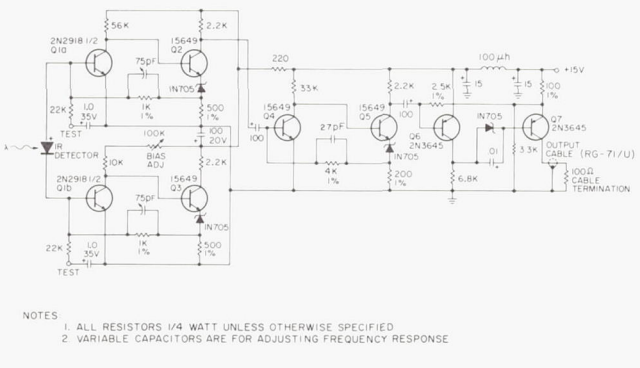

NOTES
1. ALL RESISTORS 1/4 WATT UNLESS OTHERWISE SPECIFIED
2. VARIABLE CAPACITORS ARE FOR ADJUSTING FREQUENCY RESPONSE

Figure 25.- Low-impedance amplifier for solid-state infrared detectors.

The input stage of the amplifier is a differential input and is dc coupled to the detector. The bias on the detector, that is, the voltage between input stages, can be adjusted

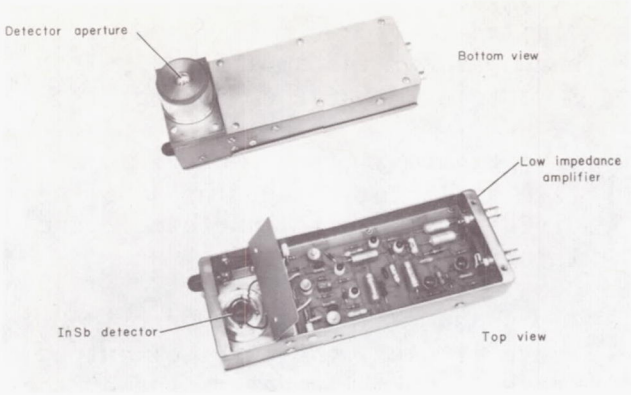

Figure 26.- Infrared radiometer.

to zero with the variable resistor in the collector circuit of one of the input stages (shown in fig. 25 as "bias adjust"). Because of the low input impedance of the amplifier, the bias does not vary appreciably during the time the radiation signal is present.

The amplifier is a pulse amplifier and is designed to have a wider dynamic range for a positive polarity signal going to Q1a. Therefore, one must insure that the positive lead of the detector is connected to Q1a. When calibrating the detector with a modulated radiation signal, the output voltage into a 100 Ω load must not exceed 0.4 V peak-to-peak in order to avoid saturating the amplifier. For normal single-pulse operation the output voltage can reach 4.0 V into a 100 Ω load before saturation.

The noise output is due primarily to current produced by the differential input stage of the amplifier. This noise current is dependent on the impedance between the input terminals and, therefore, on the particular detector. Noise levels observed by InSb detectors with flakes of approximately 1 by 1 mm were from 2 to 8 mV.

To prevent the amplifier from ringing on a fast-rising input pulse, small compensating capacitors are required in parallel with the feedback resistors, as indicated in figure 25. The value of these capacitors depends on the particular detector being used. To determine this value, a fast-rising radiation pulse should be fed into the detector (via the GaAs light emitting diode described earlier, for example), and the capacitors adjusted until the ringing is minimized.

APPENDIX C

DETECTOR NOISE LIMITATIONS

Often a ballistic-range or shock-tube experiment requires accurate measurement of very low power sources. Some noise source is inherent in any radiometer design, and eventually it obscures a low-level signal, thus placing a lower limit on the source power which can be measured. It will be shown that this lower limit is a function of the precision required and the measurement time interval. The lowest source limit for any radiometer is achieved when the dominant noise is that from the inherently random arrival of photons at the detector from the source being measured. When the number of photons that are incident on the detector during the measurement time interval becomes small, the degree of precision to which measurement can be made is decreased. Multiplier phototubes approach this limit. Additional noise from the incident photon flux is observed when IR detectors are used. These detectors respond to the ambient IR emission from the room-temperature background, or from the filter before the detector. Indeed, there is always ambient incident radiation on any detector, but the contribution to the noise from the ultraviolet and visible (the photocathode regime) emission is negligible. With either detector, the noise is increased after the subsequent conversion of the photon flux to a current, and after the amplification of that current to a value adequate to be measured by conventional oscilloscopes. The resulting test signal of interest is compared to the final noise, and the ratio is termed the signal-to-noise ratio (abbreviated S/N hereinafter). This definition will subsequently be made precise.

Noise sources of radiometers that are used to measure short duration signals will be discussed in this appendix. As has been implied before, the noise sources of interest are not necessarily the same for multiplier phototubes as for IR detectors, and the following treats the cases separately.

MULTIPLIER PHOTOTUBES

The electron multiplication within a multiplier phototube permits large amplification of the photoemissive current while adding little noise. In fact, when low-level signals are being measured by high multiplier gain within the tube, the observed noise consists of variations in the photoemissive current that have been increased slightly by the multiplication process. It can easily be shown that for high-frequency applications, the multiplier phototube dark-current noise is negligible. Subsequent amplifier and recording system noise should be unimportant in a well-designed system. Multiplier-phototube noise is well documented in the literature and may be reviewed in references 11, 13, and 36 through 41, which also include extensive reference lists.

If the photoemissive current, i, is thought of as a random variable, we can define S/N of i as

$$\left(\frac{S}{N}\right)_i \equiv \frac{\bar{i}}{E_{rms}} = \frac{\int_0^\infty iP(i)di}{\left[\int_0^\infty (i - \bar{i})^2 P(i)di\right]^{1/2}} \tag{C1}$$

where $\bar{i}$ is the mean of i, E_{rms} is the root-mean-square error of i about the mean, and P(i) is the probability law for i.

If we assume that i results from a series of independent events (i.e., the arrival of electrons at the first dynode in a short interval of time, δt) then P(i) becomes a Poisson probability law (see ref. 42), and we have

$$\left(\frac{S}{N}\right)_i = \sqrt{N_e} \tag{C2}$$

where N_e is the mean number of electrons contained in the measurement time interval. The mean photoemissive current, in electrons per second, is the integrated product of the mean incident photon "current" and the quantum efficiency of the multiplier phototube cathode. Cathode quantum efficiencies of some tubes are as high as 0.2 electron per photon in their most efficient range (see ref. 11, p. 88), so that the $(S/N)_i$ given by the above equation might be as much as 45 percent (i.e., square root of the quantum efficiency) of the S/N of the incident photon "current."

The assumption which was made above of independence of the arrival of electrons at the first dynode is a simplification of the actual situation. There are, however, slight attractive interactions between the photons arriving at the cathode and slight repulsive interactions between the resulting electrons as they leave the cathode. However, if the source is incoherent, this assumption is acceptably accurate for the evaluation of the degree of noise to expect from a proposed experiment.

The noise added by the electron multiplication is given by the noise factor, $n_f = m/(m - 1)$, where m is the gain per stage. Typical values for the noise factor for 10-stage tubes are 2 to 1.3 for overall electron gains of 10^3 to 10^6 (corresponding to gain per stage of 2 to 4). For the present purpose, 2 will be used as an approximate value. Thus, at the multiplier-phototube output, S/N is decreased, and equation (C2) becomes (see ref. 36)

$$\left(\frac{S}{N}\right)_{output} = \sqrt{\frac{N_e}{2}} \tag{C3}$$

If the time interval during which the measurement is to be made is δt, in seconds, then

$$N_e = \frac{\bar{i}\delta t}{e} \cong 6\times10^{18}\bar{i}\delta t \tag{C4}$$

where e is the electron charge, and $\bar{i}$ is in amperes. During δt, the signal-to-noise ratio at the multiplier-phototube output is given by

$$\left(\frac{S}{N}\right)_{output} = \sqrt{\frac{\bar{i}\delta t}{2e}} \cong \sqrt{3\times10^{18}\ \bar{i}\delta t} \tag{C5}$$

The time resolution interval, δt, is a fundamental parameter of the experiment design; however, this quantity must be interpreted in terms of electronic amplifier characteristics (i.e., rise time, time constant, or band pass). The relationship of δt to these parameters is somewhat arbitrary. Often the choice is to take the electronic rise time, τ_r, to be equal to the time interval to be resolved. When this is done, an approximate expression can be obtained that relates $(S/N)_{output}$ to the amplifier frequency response. The rise time and frequency response are related by

$$\tau_r \cong \frac{1}{3\Delta f} \tag{C6}$$

where Δf is the electronic band pass of the system. Equation (C5) becomes

$$\left(\frac{S}{N}\right)_{output} \cong \sqrt{\frac{\bar{i}}{6e\Delta f}} \tag{C7}$$

An exact expression in terms of the electronic band pass is given in reference 13; it is modified here to include the noise factor, and is

$$\left(\frac{S}{N}\right)_{output} = \sqrt{\frac{\bar{i}}{2n_f e\Delta f}} \tag{C8}$$

The mean cathode current is given by

$$\bar{i} = A\int_0^\infty H(\lambda)T(\lambda)\mathcal{E}(\lambda)d\lambda,\ A \tag{C9}$$

where

A area of the radiometer aperture, cm^2

$H(\lambda)$ radiant flux incident on the aperture

$T(\lambda)$ transmission of the optical components between the aperture and the cathode

$\mathcal{E}(\lambda)$ quantum efficiency of the cathode

Equations (C7) and (C9) permit the calculation of S/N for a specified test condition. Alternatively, the equations define a minimum measurable signal for a specified minimum $(S/N)_{output}$. As an example, consider the measurement of the strength of the Na doublet at 0.589 μ, from the shock region of a blunt model flying in a ballistic range. The radiometer will be presumed to have an electronic rise time of 0.1×10^{-6} second and to consist of an S-20 multiplier phototube, a spectral filter passing 20-percent of the Na line, and an aperture of 1 cm^2 that is positioned 1 m from the flight path. If the minimum acceptable $(S/N)_{output}$ is 10, then equation (C9) becomes

$$\bar{i} = (1\ cm^2)I(0.20)(3.5\times10^{-2}A/W) = 0.007\ I,\ A$$

where I is the irradiance on the aperture, W/cm^2 (see eq. (8)), and the approximate value for $\mathcal{E}(\lambda)$ was obtained from reference 12. Using equation (C6), equation (C7) becomes:

$$10 \cong \sqrt{\frac{0.007\ I}{(6)(1.6\times10^{-19})(3.3\times10^{6})}}$$

or $I = 5\times10^{-8}$ W/cm^2 incident on the radiometer aperture.

Since the detector subtends $(1/100)^2$ steradians, we arrive at the minimum source strength of 5×10^{-4} W/sr toward the radiometer that is detectable with a $(S/N)_{output}$ greater than 10.

SOLID-STATE INFRARED DETECTORS

The noise observed in the output current of a cooled solid-state infrared detector is the result of several statistical processes; that is, the incident radiation, the generation and recombination of electron-hole pairs, and the leakage of current within the detector material. There is some disagreement on what part of the resulting noise is due to each process (ref. 43); however, for our purpose, it is possible to consider the noise in the output current as an inherent property of the current that depends only on its magnitude, as was the case for multiplier photototubes. This is proper if all the radiation incident on the detector emanates from incoherent sources (ref. 43). The mean output current from an infrared detector is then

$$\bar{i}_\phi = \bar{i}_v + \bar{i}_b \qquad \text{(C10)}$$

where $\bar{i}$ is the mean current generated by the test event and $\bar{i}_b$ is the mean current generated by background radiation in the view field of the detector.

The mean square noise in this current is given by (ref. 44):

$$(E_{rms})^2 = 2(\bar{i} + \bar{i}_b)e\Delta f \tag{C11}$$

For detection of weak signals, we have

$$\bar{i} \ll \bar{i}_b \tag{C12}$$

and equation (C11) becomes

$$(E_{rms})^2 = 2\bar{i}_b e\Delta f \tag{C13}$$

Dividing the root-mean-square noise into the signal current, we have the maximum S/N attainable for an infrared detector

$$\left(\frac{S}{N}\right)_{MAX} = \frac{\bar{i}}{E_{rms}} = \frac{\bar{i}}{\sqrt{2\bar{i}_b e\Delta f}} \tag{C14}$$

The current generated by the background may be approximated by assuming a value of unity for the detector quantum efficiency. We then have $\bar{i}_b = AH_b e$ where A is the detector area in cm^2, and H_b is the background irradiance in photons/cm^2-sec. The background-induced current can be reduced by cooling the background (with dry ice, for example). If a narrow-pass filter is used in conjunction with the detector, it becomes all or part of the background. To illustrate this, consider an InSb detector with an area of 0.04 cm^2, with a hemispherical field of view, and which views a background of emissivity of 1 from 1.0 to 5.5 μ, first at room temperature, and then at dry ice temperature.

(1) Room temperature, 297° K, $H_b \cong 2.4\times10^{16}$ photons/cm^2-sec

$$\bar{i}_b \cong (4\times10^{-2})(2.4\times10^{16})(1.6\times10^{-19}) \cong 1.5\times10^{-4} \text{ A}$$

(2) Dry ice temperature, 195° K, $H_b \cong 1.5\times10^{14}$ photons/cm^2-sec

$$\bar{i}_b \cong (4\times10^{-2})(1.5\times10^{14})(1.6\times10^{-19}) \cong 9.6\times10^{-7} \text{ A}$$

In practice, the (S/N) for a given radiometer is somewhat less than that given by equation (C14). If a conventional voltage amplifier is used, input Johnson noise is added (see ref. 14), and the signal-to-noise ratio becomes

$$\left(\frac{S}{N}\right)_{output} = \frac{\bar{i}}{\sqrt{2\bar{i}_b e\Delta f + \frac{4kT\Delta f}{R}}} \tag{C15}$$

where R is the Johnson noise resistance (usually greater than the amplifier-input impedance by a factor of 2 or 3), T is the temperature, and k is Boltzmann's constant.

The current amplifier discussed in appendix B is an operational amplifier that employs negative feedback to achieve a low input impedance. The capacitance and resistance of the detector have an influence on the feedback network, in turn, which affects the resulting noise. The amplifier noise is therefore dependent on the particular detector and is difficult to calculate. Suffice it to say that for the amplifier described, and using commercially available InSb detectors with flake sizes of about 0.04 cm^2, the noise contribution due to the amplifier was relatively small, and resulted in a (S/N) of about half that given by equation (C14).

ADVANTAGE OF MULTIPLIER PHOTOTUBES

In the infrared response region of the photocathode surface, the quantum efficiency is very low. There are available for use in this spectral region an assortment of solid-state photodiodes with quantum efficiencies near 1 electron per photon (see, e.g., ref. 45). The question arises as to when the low quantum efficiency of the photocathode offsets the advantage of the low-noise electron amplification to such an extent that the solid-state photodiode produces a greater signal-to-noise ratio. The following analysis of this question is based on an analysis given in reference 13.

Consider a low level of monochromatic irradiance to be measured first by a multiplier phototube and second by the solid-state photodiode. Figure 27 depicts the two cases. We have directly the average currents from the detectors,

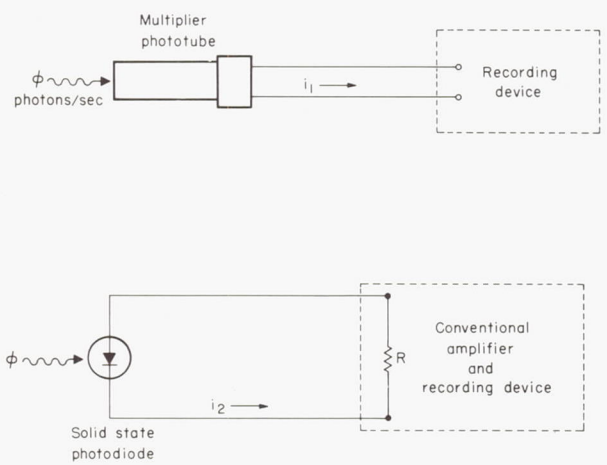

Figure 27.- Circuits defining i_1 and i_2 used in discussion of noise.

$$\left.\begin{aligned} \overline{i}_1 &= Q_1 \phi e \\ \overline{i}_2 &= Q_2 \phi e \end{aligned}\right\} \quad \text{and} \qquad \text{(C16)}$$

where Q_1 and Q_2 are the quantum efficiencies of the photocathode and the solid-state photodiode, respectively, expressed in electrons per photon. Using equation (C8) we can write for the multiplier phototube

$$\left(\frac{S}{N}\right)_1 \cong \sqrt{\frac{\overline{i}_1}{4e\Delta f}}$$

where we have taken $n_f = 2$ as above.

Rewriting, we get

$$Q_1 \phi e \cong 4e\Delta f\left[\left(\frac{S}{N}\right)_1\right]^2 \tag{C17}$$

If the solid-state photodiode is to be considered for replacement of a multiplier phototube, then it should be insensitive to background irradiance at wavelengths longer than about 1.2 μ. If this is the case, equation (C12) does not apply, as the background irradiance would be less than about 10^{-3} photons/μsec/cm^2. The resulting noise in i_2 is then Johnson noise and equation (C15) reduces to

$$\left(\frac{S}{N}\right)_2 \cong \frac{\overline{i}_2}{\sqrt{\frac{4kT\Delta f}{R}}}$$

Rewriting, using equation (C16), and dividing the result by equation (C17), we get

$$X = \frac{\left(\frac{S}{N}\right)_1}{\left(\frac{S}{N}\right)_2} \cong \frac{Q_1}{Q_2}\,\frac{1}{\left(\frac{S}{N}\right)_1}\,\frac{1}{2e}\,\sqrt{\frac{kT}{R\Delta f}} \tag{C18}$$

where X represents the improvement in signal-to-noise ratio of the multiplier phototube over the photodiode. For a conventional amplifier (see, ref. 13)

$$\Delta f \cong \frac{1}{2\pi RC}$$

where C is the input capacitance expressed in farads. We then obtain

$$X \cong \frac{Q_1}{Q_2}\,\frac{1}{\left(\frac{S}{N}\right)_1}\,\frac{1}{2e}\,\sqrt{2\pi kC} = 3.5\times10^8\,\frac{Q_1}{Q_2}\,\frac{1}{\left(\frac{S}{N}\right)_1}\,\sqrt{C}$$

where the coefficient is evaluated for $T = 300°$ K. Taking $C = 20$ μμF, and $Q_2 = 1.0$, we have

$$X \cong 1.5\times10^3\,\frac{Q_1}{(S/N)_1} \tag{C19}$$

If the lowest acceptable S/N ratio is specified, then Q_1, which gives equal signal-to-noise ratios for each detector, can be obtained from (C19) by setting X equal to 1.

Cathode quantum efficiencies greater than these values result in an improvement in S/N when a multiplier phototube is used. The following table lists values of S/N and Q_1 for X = 1.

S/N	Cathode quantum efficiencies for X = 1, electrons/photon
1	0.00067
3	.002
10	.0067

IMPROVEMENT OF SIGNAL-TO-NOISE RATIO

As can be seen from equations (C8) and (C14), the S/N can be improved by decreasing the time resolution of the data (increasing τ_r), or by increasing the mean signal current, $\bar{i}$.

The oscillograms in figure 28 qualitatively illustrate the effects of τ_r on $(S/N)_{output}$. The traces were made by mechanically modulating at 270 Hz, a low-level irradiance on a radiometer and displaying the signal before, during, and after the radiation pulses. The radiometer consisted of a multiplier phototube and an amplifier (fig. 24). The upper trace was made while the full frequency response of the amplifier and oscilloscope was utilized (about 5 MHz, or a rise time of about 0.08 μsec). The noise when irradiance is present is due to statistical variation of current within the multiplier phototube. The lower trace shows the change in noise when τ_r is increased to 20 μsec by adding a capacitor to the multiplier-phototube anode (see fig. 23). The resulting rise time is 2.3 RC, where R is the input impedance of the amplifier. Thus, it is seen that the noise may be decreased for display purposes if time resolution broadening can be afforded in the data.

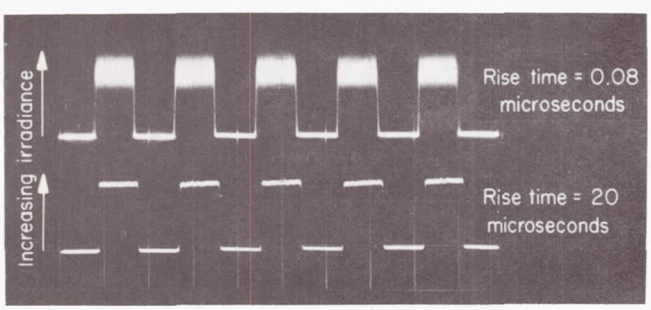

Figure 28.- Outputs from a multiplier-phototube radiometer irradiated with the same chopped low level source.

The signal current can be increased by several means to improve the $(S/N)_{output}$, for example, by choosing a detector with higher quantum efficiency, or increasing the radiation to the photocathode, which may be achieved by moving the radiometer closer to the source or by utilizing improved collection optics. In the case of a monochromator with a given spectral resolution, the maximum radiation to the photocathode is with the slit widths equal. Other techniques that increase the effective efficiency of a multiplier-phototube cathode by multiple reflection are discussed in references 46 and 47.

APPENDIX D

STANDARD LAMP-CURRENT ACCURACY REQUIREMENTS

The emission from standard tungsten lamps (used for radiometer calibration) is exceedingly sensitive to the operating current. The required accuracy of current measurement is derived below, in terms of the desired calibration accuracy. The derivation is based on relating radiant power from the lamp to the electrical power driving the lamp.

The spectral radiance from a tungsten lamp filament is given by the following equation:

$$E(\lambda,T) = \varepsilon(\lambda,T)W(\lambda,T) \tag{D1}$$

where

$E(\lambda,T)$ spectral radiance, $W/cm^2\text{-}\mu$

$\varepsilon(\lambda,T)$ emissivity of tungsten

λ wavelength, μ

T filament temperature, °K

and

$$W(\lambda,T) = \frac{C_1}{\lambda^5\left(\exp\frac{C_2}{\lambda T} - 1\right)}, \ W/cm^2\text{-}\mu \tag{D2}$$

which is Planck's blackbody equation, with C_1 equal to 37,413 $W\text{-}\mu^4/cm^2$ and C_2 equal to 14,400 μ-°K. From equation (D1) the result is immediately obtained that

$$\frac{\partial E}{\partial T} = \frac{C_1\varepsilon}{\lambda^5}\left(\exp\frac{C_2}{\lambda T} - 1\right)^{-2}\frac{C_2}{\lambda T^2}\exp\frac{C_2}{\lambda T} + E\frac{\partial \ln\varepsilon}{\partial T} \tag{D3}$$

Note that for $\lambda < 1\ \mu$ and $T < 3000°$ K we have

$$\exp\frac{C_2}{\lambda T} >> 1 \tag{D4}$$

Also, from data shown in reference 22, it was derived that

$$\left|\frac{\partial \ln\varepsilon}{\partial T}\right| << \frac{C_2}{\lambda T} \tag{D5}$$

The data of this reference are for temperatures from 1600° to 2800° K. Using inequalities (D4) and (D5), we rewrite equation (D3) as

$$\frac{\partial E}{\partial T} = E \frac{C_2}{\lambda T^2} \tag{D6}$$

The above expression describes the change of specific radiance that results from filament temperature change.

The total power radiated from the lamp filament is related to the input electrical power in the following equation:

$$i^2 R = \xi \bar{\varepsilon} \sigma T^4 A \tag{D7}$$

where

i lamp current, A

R filament resistance, Ω

ξ inverse filament efficiency, assumed to be a constant

$\bar{\varepsilon}$ total emissivity of tungsten

σ Stefan-Boltzmann constant, $W/cm^2\text{-}°K^4$

A radiating area, cm^2

From equation (D7) it is obtained that

$$2iR \frac{\partial i}{\partial T} + i^2 \frac{\partial R}{\partial T} = k\bar{\varepsilon} T^3 \left(4 + \frac{\partial \ln \bar{\varepsilon}}{\partial \ln T}\right) \tag{D8}$$

where

$$k = \xi \sigma A$$

From the results of reference 48 it was also derived that $\partial \ln \bar{\varepsilon} / \partial \ln T << 4$; thus,

$$2iR \frac{\partial i}{\partial T} + i^2 \frac{\partial R}{\partial T} = 4\, k\bar{\varepsilon} T^3 \tag{D9}$$

Rearranging equation (D9) and substituting in equation (D7), we get

$$\frac{T}{i} \frac{\partial i}{\partial T} = 2 - \frac{T}{2R} \frac{\partial R}{\partial T} \tag{D10}$$

Note that

$$\frac{\partial R}{\partial T} = \frac{R}{\rho}\frac{\partial \rho}{\partial T}$$

where ρ is the resistivity of tungsten, ohm-cm, and equation (D10) becomes

$$\frac{T}{i}\frac{\partial i}{\partial T} = 2 - \frac{T}{2\rho}\frac{\partial \rho}{\partial T} \tag{D11}$$

Combining equations (D11) and (D6), we get

$$\frac{E}{i}\frac{\partial i}{\partial E} = \left(2 - \frac{T}{2\rho}\frac{\partial \rho}{\partial T}\right)\frac{T}{C_2}\lambda \tag{D12}$$

An equation fitted to the resistivity data of reference 48 is,

$$\rho = -1.0\times10^{-5} + 3.37\times10^{-8}\ T \tag{D13}$$

for T greater than 1000° K. Substituting equation (D13) into equation (D12), and replacing $\partial E/\partial i$ by $\delta E/\delta i$ to represent actual small errors, we get

$$\frac{\delta i}{i} = \frac{(T - 396)}{(T - 297)}\left(\frac{\lambda T}{9.6\times10^3}\right)\frac{\delta E}{E} \cong \frac{\lambda T}{10^4}\frac{\delta E}{E} \tag{D14}$$

where $\delta E/E$ and $\delta i/i$ are fractional errors in spectral radiant output and current, respectively. Equation (D14) relates the accuracy in lamp current to the accuracy in the spectral radiance.

For verification, a strip-filament lamp and a coiled-filament lamp of the types described in this report were operated under various conditions. The ratio of fractional change in current to the fractional change in radiance was compared to that calculated by the approximate form of (D14), as follows:

Lamp filament	[1]T, °K	λ, μ	$(\delta i/i)/(\delta E/E)$ Calculated	$(\delta i/i)/(\delta E/E)$ Measured
Strip	2200	0.38	0.083	0.097
Coiled	2900	.38	.11	.14
Coiled	2900	.25	.072	.094

Note that at short wavelengths the lamp-radiance accuracy is of the order of 0.1 of the current accuracy.

---

[1]These temperatures were deduced from color temperatures measured with an optical pyrometer and are, therefore, only approximate for the coiled-filament lamp.

The above data show that equation (D14), although approximate, is adequate for determining the degree of precision to expect from the standard lamps described in this report when the operating conditions - specifically the accuracy of current regulation and the metering apparatus that is used - are described.

REFERENCES

1. Allen, H. Julian; Seiff, Alvin; and Winovich Warren: Aerodynamic Heating of Conical Entry Vehicles at Speeds in Excess of Earth Parabolic Speed. NASA TR R-185, 1963.

2. Craig, Roger A.; and Davy, William C.: Thermal Radiation From Ablation Products Injected Into a Hypersonic Shock Layer. NASA TN D-1978, 1963.

3. Stephenson, Jack D.: Measurement of Optical Radiation From the Wake of Ablating Blunt Bodies in Flight at Speeds Up to 10 Km Per Second. NASA TN D-2760, 1965.

4. Seiff, Alvin: Ames Hypervelocity Free Flight Research. Astronautics and Aerospace Engr., vol. 1, no. 11, Dec. 1963, pp. 16-23.

5. Kantrowitz, Arthur: The Shock Tube and Plasma Dynamics. J. Environ. Sci., vol. 9, June 1966, pp. 13-17.

6. Wood, Allen D.; and Andrews, J. C.: Fast-Response Total Thermal Radiation Detectors. Proc. 2nd Intl. Congress on Instrumentation in Aerospace Simulation Facilities, Stanford University, Aug. 29-31, 1966, pp. 13.1-13.13.

7. Kruse, Paul W.; McGlauchlin, Laurence D.; and McQuistan, Richmond B.: Elements of Infrared Technology, Generation, Transmission and Detection. John Wiley and Sons, Inc., 1962.

8. Arnold, J. O.: A Shock Tube Determination of the Electronic Transition Moment of the C_2(Swan) Bands. JQSRT, vol. 8, no. 11, 1968, pp. 1781-94.

9. Jenkins, F. A.; and White, H. E.: Fundamentals of Optics. Third ed., McGraw-Hill Book Co., 1957.

10. Pollack, S. A.: Angular Dependence of Transmission Characteristics of Interference Filters and Applications to a Tunable Fluorometer. J. Appl. Optics, vol. 5, no. 11, Nov. 1966, pp. 1749-56.

11. Anon.: Phototubes and Photocells. RCA Technical Manual, PT 60, Radio Corp. Am., Lancaster, Pa., 1963.

12. Anon.: Dumont Multiplier Phototubes. Third ed., Dumont Laboratories, Div. of Fairchild, Clifton, N. J., March 1963.

13. Lallemand, A.: Photomultipliers. Astronomical Techniques. Chapter 6, William A. Hiltner, ed., Chicago Press, Chicago, Ill., 1962.

14. Slawek, J. E., Jr.: The Photovoltaic Indium Antimonide Infrared Detector. Davers Corp., Horsham Valley Industrial Center, Horsham, Pa.

15. Kovit, Bernard: Infrared Detectors, New Designs, New Applications. Space/Aeronautics, vol. 36, no. 4, part 1, Nov. 1961, pp. 104-107.

16. Mayers, D. F.: Singular and Non-Linear Integral Equations. Numerical Solutions of Ordinary and Partial Differential Equations. Chapter 14, L. Fox, ed., Addison-Wesley Pub. Co., Palo Alto, Calif., 1962.

17. Johnston, R. G.; and Madden, R. P.: On the Use of Thermopiles for Absolute Radiometry in the Far Ultraviolet. Appl. Optics, vol. 4, no. 12, Dec. 1965, pp. 1574-1580.

18. Eisenman, W. L.; Bates, R. L.; and Merriam, J. D.: Black Radiation Detector. J. Opt. Soc. Am., vol. 53, no. 6, 1963, pp. 729-734.

19. Kostkowski, H. J.; Erminy, D. E.; and Hattenberg, A. T.: New Spectral Radiance Calibrations. J. Opt. Soc. Am., vol. 54, no. 11, Nov. 1964, p. 1386.

20. Samson, James A. R.: Absolute Intensity Measurement in the Vacuum Ultraviolet. J. Opt. Soc. Am., vol. 54, no. 1, Jan. 1964, p. 6.

21. Compton, D. L.: Measurements of Ultraviolet (575 Å - 1800 Å) Radiation From Nitrogen at Temperatures From 13,000° K to 16,000° K. AIAA Paper 66-422, 1966.

22. De Vos, J. C.: A New Determination of the Emissivity of Tungsten Ribbon. Physica, vol. 29, no. 10, Oct. 1954, pp. 690-714.

23. Rutgers, G. A. W.; and De Vos, J. C.: Relation Between Brightness Temperature, True Temperature and Colour Temperature of Tungsten. Luminance of Tungsten, Physica, vol. 20, no. 10, Oct. 1954, pp. 715-720.

24. Stair, Ralph; Johnson, Russell G.; and Halback, E. W.: Standard of Spectral Radiance for the Region of 0.25 to 2.6 Microns. J. Res. Natl. Bur. Stds., A. Physics and Chemistry, vol. 64A, no. 4, July-August 1960, pp. 291-296.

25. Stair, Ralph; Schneider, William E.; and Jackson, John K.: A New Standard of Spectral Irradiance. Appl. Optics, vol. 2, no. 11, Nov. 1963, pp. 1151-1154.

26. Zubler, E. G.; Mosby, F. A.: An Iodine Incandescent Lamp With Virtually 100 Per Cent Lumen Maintenance. Illuminating Engineering, vol. 54, no. 12, Dec. 1959, pp. 734-739.

27. Dostal, Frank: Light Light Choppers. Optical Spectra, vol. 2, no. 2, March-April 1968, pp. 29-32.

28. Moore, R. D.: Lock-In Amplifier for Signals Buried in Noise, Electronics. June 8, 1962, pp. 40-43.

29. Pruett, G. R.; and Petritz, R. L.: Detectivity and Preamplifier Considerations for Indium Antimonide Photovoltaic Detectors. Proc. IRE, Paper 4.1.9, vol. 47, no. 9, Sept. 1959, pp. 1524-1529.

30. Whiting, E. E.: A New Four-Channel Spectrograph for Ballistic-Range Radiometry. Proc. 2nd Intl. Congress on Instrumentation in Aerospace Simulation Facilities, Stanford University, Aug. 29-31, 1966, pp. 14.1-14.5.

31. Reis, Victor H.: Oscillator Strengths for the N_2 Second Positive and N_2^+ First Negative Systems From Observations of Shock Layers About Hypersonic Projectiles. JQSRT, vol. 4, no. 6, Nov.-Dec. 1964, pp. 783-792.

32. St. Pierre, C.: Visible Emission From 1/2-In. Hypervelocity Models Measured With a Moving Target Scan Monochromator. CARDE TM AB-59, 1960.

33. Compton, Dale E.; and Cooper, David M.: Measurements of Radiative Heating on Sharp Cones. AIAA J., vol. 3, no. 1, Jan. 1965, pp. 107-114.

34. Harrison, G. R.; Lord, R. C.; and Loofbourow, J. R.: Practical Spectroscopy, Ch. 6, Prentice-Hall, Inc., 1948.

35. Strieff, M. L.; Ferrisco, C. C.: An Investigation of the Slit Function of Infrared Littrow Type Monochromator. Paper Y-3, Symp. on Molecular Spectroscopy, Ohio State Univ., 1964.

36. Eberhardt, E. H.: Noise in Multiplier Phototubes. Applications Note E8, ITT Industrial Labs., May 1, 1965.

37. Schlueter, P.: Photomultiplier Tubes for Satellite Instrumentation. Appl. Optics, vol. 6, no. 2, Feb. 1967.

38. Anderson, L. K.; and McMurtry, B. J.: High Speed Photodetectors. Appl. Optics, vol. 5, no. 10, Oct. 1966, pp. 1573-1587.

39. Sharpe, J.: Photoelectric Cells and Photomultipliers. Electronic Technology, June 1961.

40. Eberhardt, E. H.: Noise Factor Measurements in Multiplier Phototubes. Appl. Optics, vol. 6, no. 2, Feb. 1967, pp. 359-360.

41. Tusting, Robert F.; Kerns, Quentin A.; and Knudsen, Harold K.: Photomultiplier Single-Electron Statistics. IRE Trans. NS-9, no. 3, June 1962, pp. 118-123.

42. Parzen, Emanual: Modern Probability Theory and Its Applications. John Wiley and Sons, Inc., N. Y., 1960, p. 218.

43. van Fliet, K. M.: Noise Limitations in Solid State Photodetectors. Appl. Optics, vol. 6, no. 7, July 1967, pp. 1145-1169.

44. Strong, John; and Stauffer, Frederic R.: Instrumentation for Infrared Astrophysics. Ch. 12, Astronomical Techniques, William A. Hiltner, ed., Univ. of Chicago Press, 1962.

45. Fisher, Richard: P-I-N Diode Detectors for Astronomical Photometry. Appl. Optics, vol. 7, no. 6, June 1968, pp. 1079-1083.

46. Grant, George R.; Gunter, William D., Jr.; and Erickson, Edwin F.: High Absolute Photocathode Sensitivity. The Review of Sci. Instruments, vol. 36, no. 10, Oct. 1965, pp. 1511-1512.

47. Gunter, William D., Jr.: Erickson, Edwin F.; and Grant, George R.: Enhancement of Photomultiplier Sensitivity by Total Internal Reflection. Appl. Optics, vol. 4, no. 4, April 1965, pp. 512-513.

48. Goldsmith, A.; Waterman, T. E.; and Hirschhorn, H. J.: Thermophysical Properties of Solid Materials. Wright Air Development Center Tech. Rep. 58-476, vol. 1, 1960.

NASA-Langley, 1969 —— 14 A-3192